ESTCP

DEMONSTRATION REPORT

TEMTADS 2x2 Classification Redstone Arsenal, AL

Leonard Pasion
Black Tusk Geophysics, Inc.

March 2018

ESTCP Project MR-201226

REPORT DOCUMENTATION PAGE

Form Approved
OMB No. 0704-0188

1. REPORT DATE *(DD-MM-YYYY)*	2. REPORT TYPE	3. DATES COVERED *(From - To)*
31/03/2018	ESTCP Demonstration Report	9/29/2012 - 3/28/2018

4. TITLE AND SUBTITLE
TEMTADS 2x2 Classification Redstone Arsenal, AL

5a. CONTRACT NUMBER
12-C-0079

5b. GRANT NUMBER

5c. PROGRAM ELEMENT NUMBER

6. AUTHOR(S)
Leonard Pasion

5d. PROJECT NUMBER
MR-201226

5e. TASK NUMBER

5f. WORK UNIT NUMBER

7. PERFORMING ORGANIZATION NAME(S) AND ADDRESS(ES)
Black Tusk Geophysics, Inc.
2386 East Mall Suite 112A
Vancouver, BC V6T 1Z3

8. PERFORMING ORGANIZATION REPORT NUMBER
MR-201226

9. SPONSORING/MONITORING AGENCY NAME(S) AND ADDRESS(ES)
Environmental Security Technology Certification Program
4800 Mark Center Drive, Suite 16F16
Alexandria, VA 22350-3605

10. SPONSOR/MONITOR'S ACRONYM(S)
ESTCP

11. SPONSOR/MONITOR'S REPORT NUMBER(S)
MR-201226

12. DISTRIBUTION/AVAILABILITY STATEMENT
DISTRIBUTION STATEMENT A. Approved for public release: distribution unlimited.

13. SUPPLEMENTARY NOTES

14. ABSTRACT
This report describes advanced geophysical classification (AGC) processing of Time Domain Electromagnetic Multi-Sensor Towed Array Detection System (TEMTADS) 2x2 time-domain electromagnetic data collected at the Redstone Arsenal, AL. Dynamic and cued TEMTADS2x2 AGC data were acquired by CB&I at seven 100×100-foot grids throughout the Redstone Arsenal. The grids presented a range of challenging conditions in both forested and open areas, with varying degrees of subsurface infrastructure and anomaly density.

15. SUBJECT TERMS
TEMTADS 2x2 Classification, Redstone Arsenal, munitions response, UXO, UXO on land, Live demonstration site, sensors and analysis

16. SECURITY CLASSIFICATION OF:			17. LIMITATION OF ABSTRACT	18. NUMBER OF PAGES	19a. NAME OF RESPONSIBLE PERSON
a. REPORT	b. ABSTRACT	c. THIS PAGE			Leonard Pasion
UNCLASS	UNCLASS	UNCLASS	UNCLASS	42	19b. TELEPHONE NUMBER *(Include area code)* 604-428-3382

Executive Summary

This report describes advanced geophysical classification (AGC) processing of Time Domain Electromagnetic Multi-Sensor Towed Array Detection System (TEMTADS) 2x2 time-domain electromagnetic data collected at the Redstone Arsenal, AL. Dynamic and cued TEMTADS2x2 AGC data were acquired by CB&I at seven 100×100-foot grids throughout the Redstone Arsenal. The grids presented a range of challenging conditions in both forested and open areas, with varying degrees of subsurface infrastructure and anomaly density.

BTG processed all the dynamic and cued data, but was not responsible for official QC during data collection. However, we did process and internally evaluate the dynamic and cued data collected daily on the IVS. BTG created target lists from the dynamic data and performed classification on the cued data from each grid, and submitted separate dig lists for each grid to CB&I. We initially used an amplitude-based picking algorithm to select cued locations. However, a missed seed resulted from the inaccuracy of the peak amplitude location. As a result, we switched to inverting all anomalies and using source locations for defining cued locations.

Due to a limited number of available ground truth digs, it was not possible to dig all items flagged as digs on the seven submitted dig lists. Instead, CB&I decided to dig a subset of targets identified manually by both BTG and CB&I to address the objectives of their program. This included digs both before and after the stop dig point on each list. Only a limited number of targets of interest (TOI) per grid were excavated, some of which were challenging from a classification perspective. The report closes with a review of each TOI that was intrusively investigated.

Table of Contents

List of Figures

List of Tables

Acronyms

AGC	Advanced Geophysical Classification
cm	Centimeter
BTG	Black Tusk Geophysics
CB&I	Chicago Bridge and Iron Company
CSV	Comma Separated Variable
ESTCP	Environmental Security Technology Certification Program
ISO	Industry Standard Object
m	Meter
mm	Millimeter
ms	Millisecond
MEC	Munitions and Explosives of Concern
PEDEMIS	Portable Decoupled Electromagnetic Induction Sensor
QA	Quality Assurance
QC	Quality Control
RCA	Root-Cause Analysis
ROC	Receiver Operating Characteristic
s	Second
SNR	Signal-to-Noise Ratio
TEM	Time domain Electromagnetic
TEMTADS	Time Domain Electromagnetic Multi-Sensor Towed Array Detection System
TOI	Target of Interest
UXO	Unexploded Ordnance

1 Introduction

For this study, digital geophysical mapping was performed by the cart-based Time Domain Electromagnetic Multi-Sensor Towed Array Detection System (TEMTADS 2x2). TEMTADS 2x2 data collected by CB&I were used to develop a target list of locations for cued interrogation. This report summarizes the processing carried out by Black Tusk Geophysics (BTG) on TEMTADS 2x2 cued data collected as part of this demonstration.

2 Technology description

2.1 TEMTADS 2x2

Advanced time-domain electromagnetic sensors have dramatically improved detection and classification of buried MEC. In contrast to commercial mono-static sensors such as the Geonics EM61, the multi-static geometries of next generation time domain electromagnetic sensors provide diverse excitations of a detected target. Multi-component receivers measuring the secondary field of metallic targets over multiple time channels allow for improved discrimination between thick-walled ordnance and thin-walled scrap.

The TEMTADS 2x2 (Figure 1) used for this demonstration is an advanced time domain electromagnetic sensor designed specifically for classification of MEC. The TEMTADS platform includes four transmitter loops and four 3-axis receiver antennas providing 48 independent measurements of the transient secondary magnetic field.

The TEMTADS 2x2 can be deployed in either a dynamic, full coverage mode for creating digital geophysical maps, or in a static, cued interrogation mode for interrogating individual anomalies. In dynamic mode, data are continually recorded on time channels that range from 0.025 to 2.5 ms. In cued mode, data are recorded with the TEMTADS cart stationary above a target. Cued data are recorded on time channels that range from 0.117 to 24.375 ms. In-field inversions of cued soundings help to ensure that the sensor is optimally positioned over each target.

Inversion of cued data using the TEM point-dipole model typically produces well-constrained estimates that can subsequently be input into a classification algorithm.

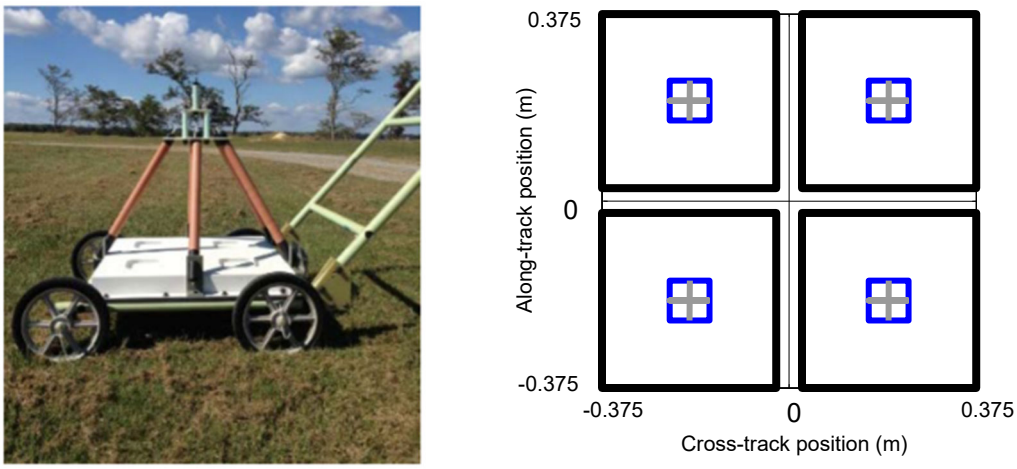

Figure 1. Left: Cued TEMTADS 2x2 array with GPS mount. Right: Sensor geometry showing four transmitters (solid black lines) and concentric 3-axis receivers. Photo credit: TEMTADS 2x2 user manual.

2.2 Detection and Classification with Advanced EMI sensors

Target detection using mono-static sensors is usually restricted to identifying anomalies that exceed a pre-defined data amplitude threshold. Data peaks are identified either along transects or off of images of gridded data. With advanced sensors, the dynamic data can be inverted for a dipole model to recover estimates of extrinsic (location, depth, and orientation) and intrinsic (dipole polarizabilities) parameters for each anomaly. Dipole source locations is more accurate than using the peak of a data anomaly for estimating target locations. In addition, properties of the estimated dipole polarizabilities can be used for anomaly screening. This process, known as "informed source selection" ISS, results in a more efficient deployment of the cued sensor, since polarizabilities are used to identify data anomalies that can be declared a non-UXO without the need for a cued interrogation measurement.

In cases where dynamic data is not of sufficient quality for classification, anomalies can be further investigated using cued interrogation data acquired over anomalies initially identified in the detection data. These cued interrogations eliminate relative positional errors by acquiring data with a stationary sensor. The multi-static, multi-component geometry of advanced sensors such as the TEMTADS 2x2 allows for reliable target characterization with a single cued sounding.

When inverting cued anomalies, the estimated polarizabilities for each recovered dipole source are matched against a pre-defined library to identify likely targets of interest (TOI) at the site. For this demonstration, all classification processing was carried out using the *UXOLab* software package developed by BTG.

3 Detection and Classification at Redstone Arsenal

3.1 Introduction

Dynamic and cued TEMTADS2x2 AGC data were acquired by CB&I at seven 100×100-foot grids throughout the Redstone Arsenal (Figure 2) between October 2015 and February 2016. The grids presented a range of challenging conditions in both forested and open areas, with varying degrees of subsurface infrastructure and anomaly density. Positioning for all grids was via Leica RTS. Grid R17 was surveyed three times, using (1) Leica RTS, (2) RTK GPS, and (3) Trimble RTS for positioning.

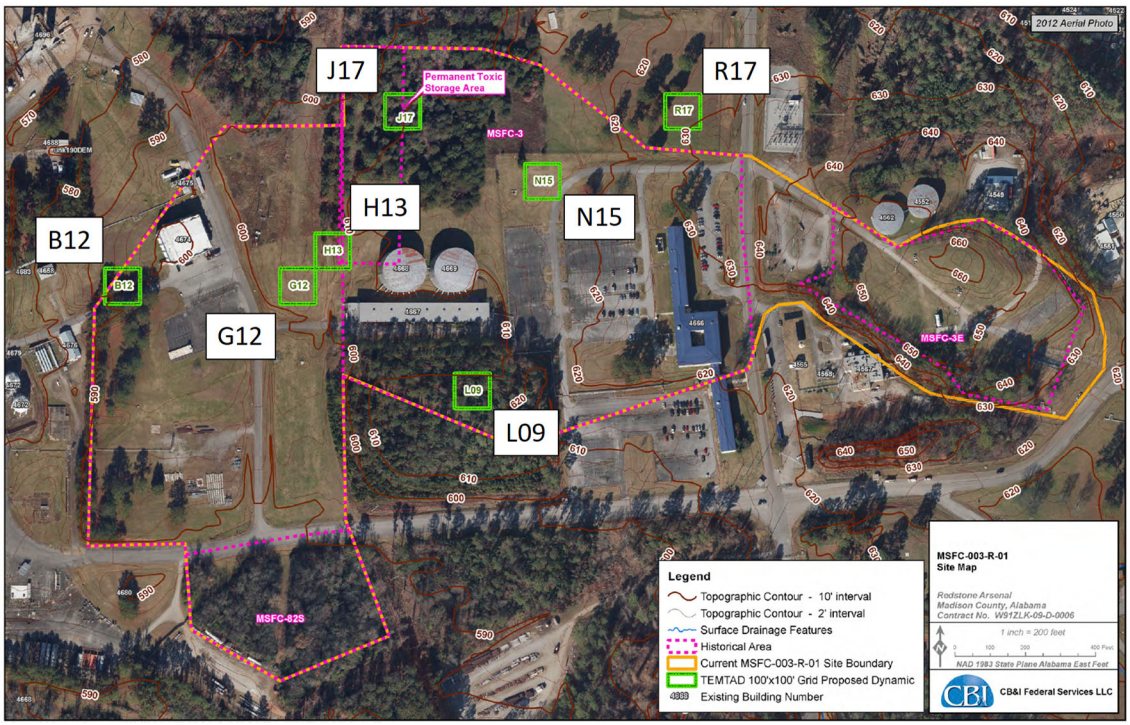

Figure 2. Redstone Arsenal, showing location of seven 100×100-foot grids (labeled green squares) within which dynamic and cued TEMTADS2x2 AGC data were collected.

BTG processed all the dynamic and cued data, but was not responsible for official QC during data collection; however, we did process and internally evaluate the dynamic and cued data collected daily on the IVS. BTG created target lists from the dynamic data and performed classification on the cued data from each grid, and submitted separate dig lists for each grid to CB&I.

3.2 Dynamic data processing

3.2.1 IVS and lag processing

The Redstone IVS comprise four large targets oriented vertically (Table 1) along an east-west line.

Table 1. Contents of Redstone instrument verification strip (IVS).

ID	Item	Depth (cm)	Orientation
IVS-1	Medium ISO)	28	Vertical
IVS-2	4.2” projectile	35	Vertical
IVS-3	Large ISO w/ bentonite	38	Vertical
IVS-4	Large ISO	38	Vertical

At each visit of the sensor to the IVS, a pair of dynamic lines directly over the targets in each direction was acquired. We used these for determining the lag associated with the RTS (or RTK GPS) positioning system. Figure 3 shows an example using data from the first day of dynamic data collection (Oct. 6, 2015). In this example the estimated positional lag (for the Leica RTS) was 0.19 s. Based on this, and other examples, for processing all dynamic data collected using the Leica RTS we applied a lag correction of 0.2 s. For data acquired in grid R17 using a Trimble RTK GPS for position, we applied a lag correction of 0.0 s. For data acquired in grid R17 using a Trimble RTS for position, we applied a lag correction of 0.3 s.

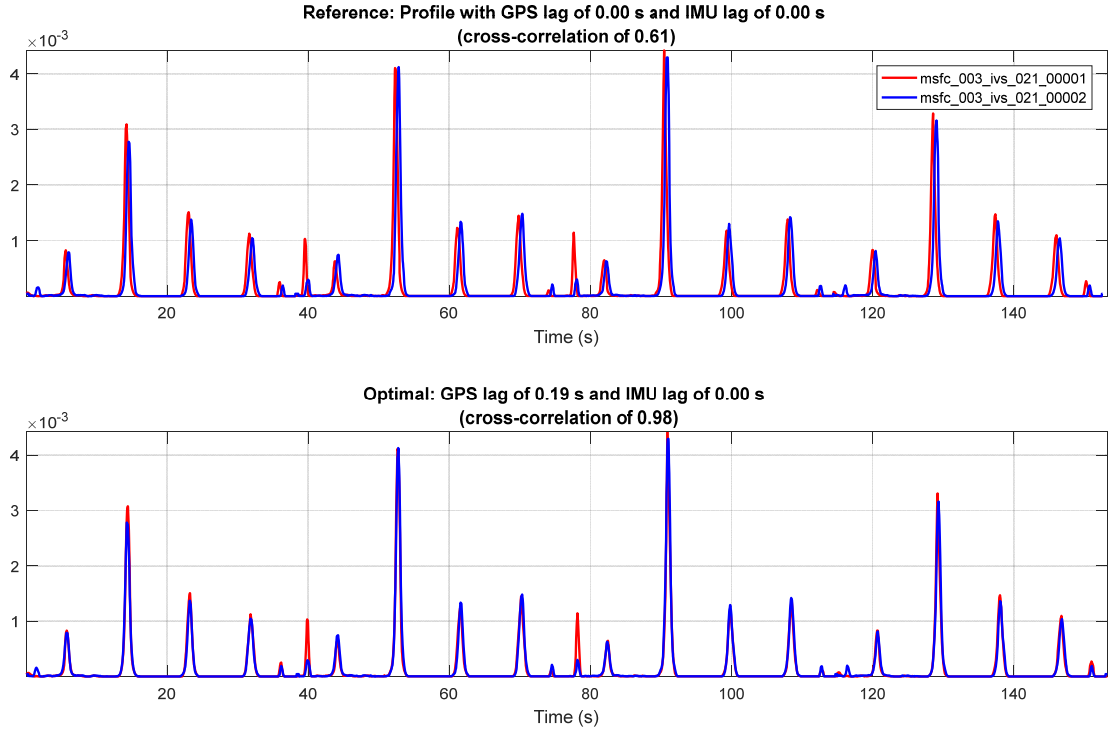

Figure 3. Example display from UXOLab's LagZilla tool showing: (top) composite of data acquired by four combinations of transmitters and receivers with no lag correction; (bottom) same, but with a lag of 0.19 s applied. Although the plot labels indicate "GPS lag", positioning in this example was via RTS. Data in this example are from Oct. 6, 2015 (PM). Note that cross-correlation increases from 0.61 to 0.98 after applying the estimated lag value.

3.2.2 Interpolating positional data

For each grid, all raw CSV files were imported into UXOLab. Data acquired using RTS positioning have an issue caused by the slower update rate of the RTS unit relative to the CPU rate of the acquisition system. Upon import into UXOLab the data are interpolated to the CPU times. This is done by interpolating the RTS positions (not the receiver positions on the cart), after which antenna corrections are applied to account for pitch, roll and heading. The RTS data are prone, especially during the start of a new line, to include points for which the recorded coordinates are very far off (e.g., many km) from the actual study area. Such data points are removed on import. Figure 4 shows an example of gridded data after import into UXOLab.

After importing data from the CSV files, additional processing is performed to improve the positional accuracy of the sensor's receivers. This addresses two issues. (1) The valid raw positional data (i.e., the unique positions) are first corrected by applying the antenna correction to account for pitch, roll and heading, then the corrected unique positional data are interpolated to the CPU times. Performing the antenna correction before interpolation of positions gives better location estimates. (2) Gaps due to shadows are interpolated. To

estimate the cart speed across the gap, logic is applied to determine whether the cart has stopped after losing RTS lock, or whether the cart kept moving at a near constant speed across the gap (based on speed estimates before and after the gap). Figure 4b shows the effect of additional processing.

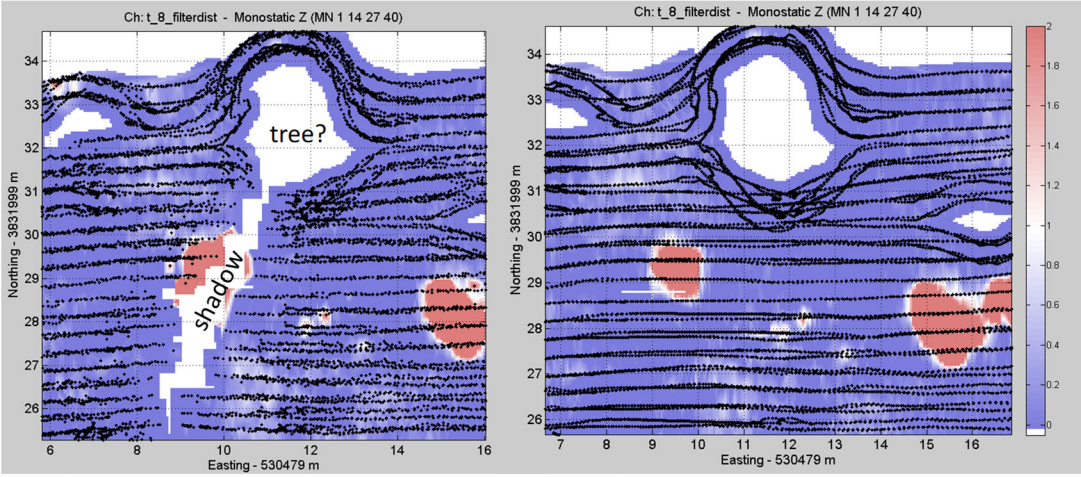

(a) Raw position data from CSV *(b) Additional processing applied*

Figure 4**.** (a) Leveled data from near the NW corner of grid L09 after import into UXOLab without additional processing. Black dots are interpolated receiver positions. The large gap at the top is presumably due to something like a tree, while the long gap extending to the SSW from the tree gap is a shadow zone caused by loss of line of sight between the RTS prism mounted on top of the cart and the laser gun at the base station. (b) Leveled data from near the NW corner of grid L09 after additional processing to improve positional accuracy. Note that the receiver tracks (black dots) are more representative of the actual tracks (i.e., high spatial frequency variation in location has been removed), and the shadow gap due to loss of line of sight between the RTS prism and laser gun is eliminated.

3.2.3 Target picking

Targets were picked using a data amplitude-based picking algorithm applied to an image of gridded data. The smallest target of interest was the MK15 WP Smoke Grenade; however, the dipole polarizability curves of the MK15 WP Smoke Grenade were not available. Instead, the polarizabilities of the MK18 Smoke Grenade, a similar walled ordnance with a fast-decaying response, were used. Because of the fast decay response, it is appropriate to use an early time channel to improve detection performance. The 8th time channel (0.214 ms) time channel was chosen for detection, as it provides a balance between being early in time to detect fast decaying targets, while being late enough in time to have reduced instrument noise.

The data at the detection channel were leveled using a 10 m-long de-median filter applied along line profiles. Within the filter window, the data points were ordered, and the upper

and lower 20% of the data were omitted when calculating the median. The leveled data were gridded using 5 cm pixels.

The target picking algorithm initially finds all peaks within the grid. A number of rules were then applied to eliminate peaks, e.g., by requiring that the threshold be exceeded by at least 3 of the 9 points centered on the peak. In addition, peaks closer than 0.3 m to a higher amplitude peak were removed. Peaks within 0.5 m were merged to the weighted average location, with weighting based on peak amplitudes. Examples of the picks for grid R17 are shown in Figure 5. Appendix 1 shows the gridded data and pick locations for all seven grids.

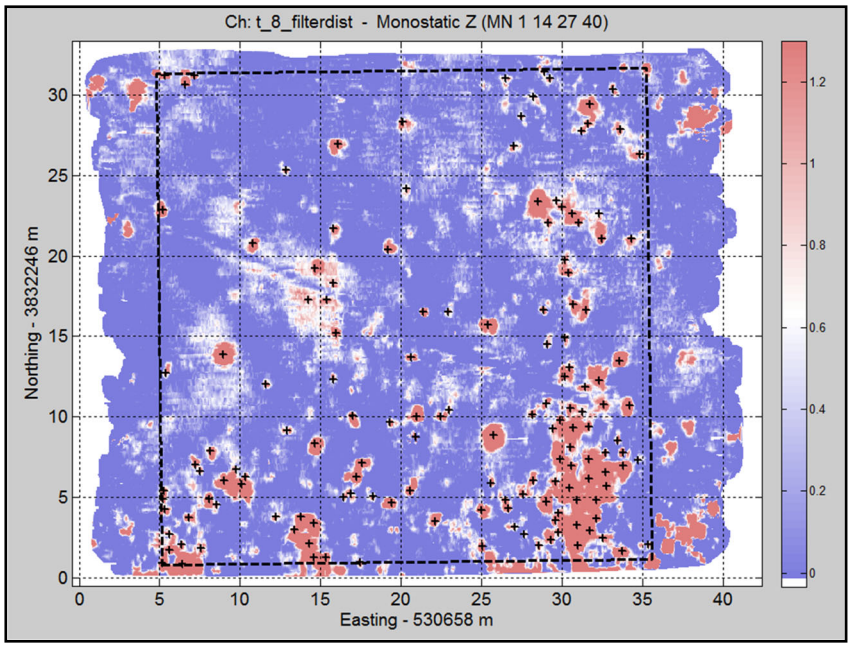

Figure 5. Gridded data (monostatic Z-component; 8th time channel = 0.214 ms) for grid R17. For this version of R17 a Leica RTS system was used for positioning. Picking threshold for this grid was 1.3. Black + symbols are target picks (149). Broken black line is grid boundary.

For each grid a noise estimate was calculated based on the average of estimates of the median absolute deviation (MAD) of the data in several relatively quiet parts of each grid. The median absolute deviation is a robust estimator of the standard deviation. In contrast to the standard deviation which takes the square root of the average of the squared deviations, the MAD sorts the absolute deviations and takes the median of these values and is less affected by large outliers. In the case that data are normally distributed, an estimate of the standard deviation is $\sigma \approx 1.4826 \times MAD$. Figure 6 includes an example of estimating the noise for Grid L09. For Grid L09, five polygons were drawn within the grid, and the MAD estimate for the regions were averaged to produce a single noise estimate number

for the grid. For the grids in this study, noise estimates varied between 0.21 for grid L09 to 3.56 for grid N15 (Table 2).

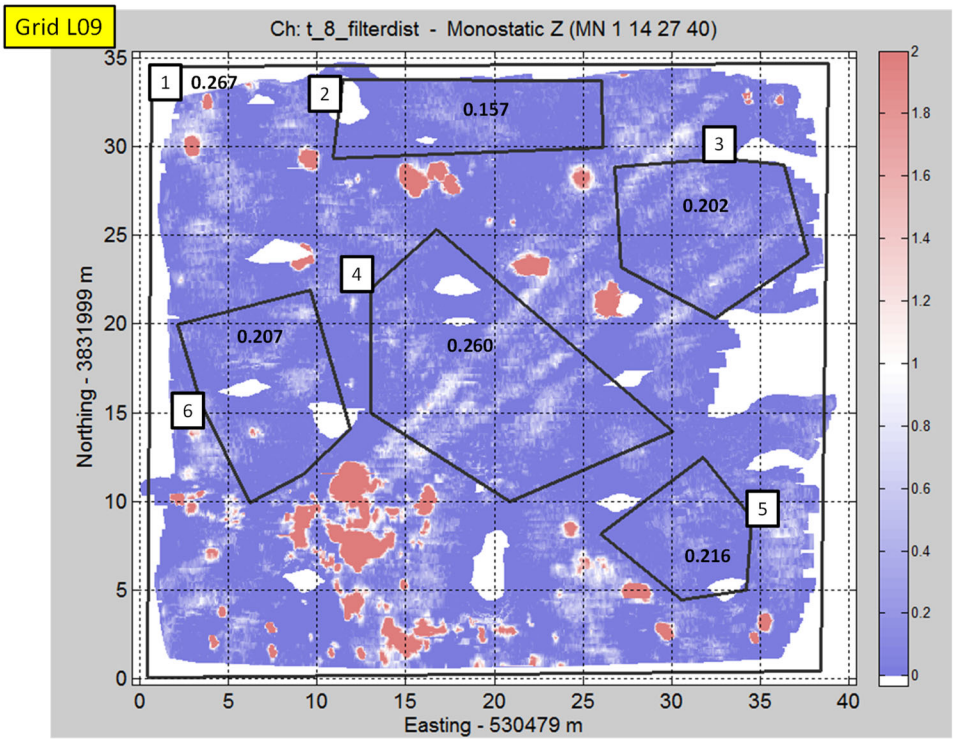

Figure 6. Example of estimating noise over a grid (L09). A number of polygons are drawn in regions where there are few anomalies. The MAD is estimated in each polygon, and the average MAD estimate is then used to calculate the standard deviation.

Table 2. Noise estimates (average median absolute deviation), picking thresholds and number of targets found in each grid. The threshold is calculated as five times the average MAD estimate of the standard deviation. Number of targets for grid R17 is based on merging picks from two versions of R17, recorded using a Leica RTS and Trimble RTK GPS for positioning.

Grid	Average MAD estimate of σ	Threshold (5 x MAD)	Number of Targets
R17 merged	0.27	1.3	153
L09	0.21	1.0	91
B12	0.92	4.6	152
N15	3.56	17.8	242
G12	0.69	3.5	238
H13	1.17	5.9	255
J17	0.50	2.5	219
Total			**1350**

Because the noise levels for all grids were too high for the stated detection threshold of the project (4.2-inch mortar at 3.1 feet below the ground surface), we instead set the detection threshold to be five times the estimated noise level. Five times the noise floor is an accepted standard for reliable detection in the UXO community. For each grid, the detection threshold was used to calculate the clearance depth for an M18 Smoke Hand Grenade and a 4.2" mortar. At depths shallower than a target's clearance depth, the target will produce an anomaly greater than the detection threshold, i.e. we expect to find all targets that are shallower than the clearance depth. Dipole polarizability values derived as part of the ESTCP ordnance library project were used to calculate target responses. For each target type, there is a range of polarizabilities corresponding to variations in target type (e.g. different Mark and Model of a particular ordnance) and non-dipolar components in the data. Table 3 lists the depths for the M18 Smoke Hand Grenade and 4.2" mortar.

Table 3. *Clearance depths corresponding to the target picking threshold.*

		Clearance Depth (m)	
Grid	**Threshold**	**M18 Hand Grenade**	**4.2" Mortar**
R17 merged	1.3	0.33	0.69
L09	1.0	0.36	0.73
B12	4.6	0.20	0.50
N15	17.8	0.08	0.33
G12	3.5	0.23	0.54
H13	5.9	0.18	0.47
J17	2.5	0.26	0.58

3.2.4 Missed seeds (target selection)

Two quality control (QC) seed items and one quality assurance (QA) seed was not included in the initial TEMTADS 2x2 derived detection list submitted for the Redstone study.

1. *Grid G12 QC Seed (530348.22, 3832110.65) m, Medium ISO, depth=0.65 m:* This seed was supposed to be a large ISO, but a medium ISO was used instead. The anomaly from a medium ISO at this depth was lower than the detection threshold.
2. *Grid H13 QA Seed (530373.59, 3832138.99) m, Medium ISO, depth=0.56 m:* The hole for this seed had collapsed, and the target was emplaced deeper than intended. As a result, this seed produced a data anomaly lower than the detection threshold.
3. *Grid B12 QC Seed (530195.89, 3832102.75) m, depth=0.3 m:* The picked location was 45 cm from the seed location, therefore exceeding the maximum allowable error of 40cm. The primary cause for the positioning error exceeding the allowable tolerance was the use of the data amplitude for target picks, rather than using inverted source locations.

3.2.4.1 Missed Seed 1. Grid G12 QC Seed

This missed seed was a medium ISO buried at a depth of 0.65 m. Not identifying the data anomaly from this seed was not considered problematic, since the target was intended to be a large ISO, but a medium ISO was mistakenly emplaced instead. In Figure 7(left), the z-component monostatic data from the 8th time channel is gridded with a maximum color scale of 3.5 mV, which is the detection threshold for Grid G12. The seed location is indicated by an 'o'. Figure 7(right) plots the same image with a maximum color scale of 1.5 mV. Figure 8 plots the profile for the 8th time channel monostatic data. The medium ISO produces a distinct data anomaly, but the anomaly falls below the target picking threshold.

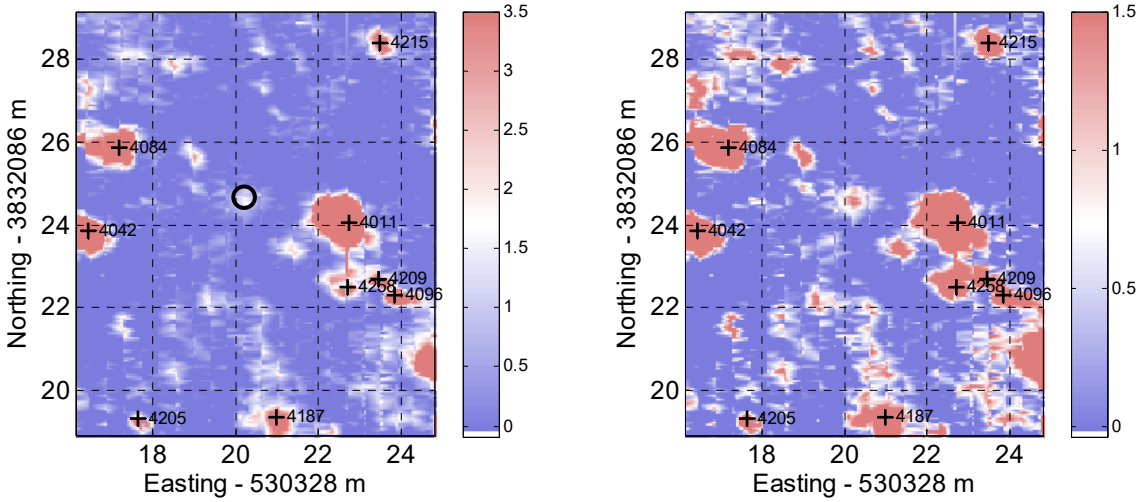

Figure 7. Gridded TEMTADS data for Missed seed 1 (Grid G12). The monostatic (i.e. coaxial) z-component data for time channel 8 is shown. Circle in plot at left shows seed location.

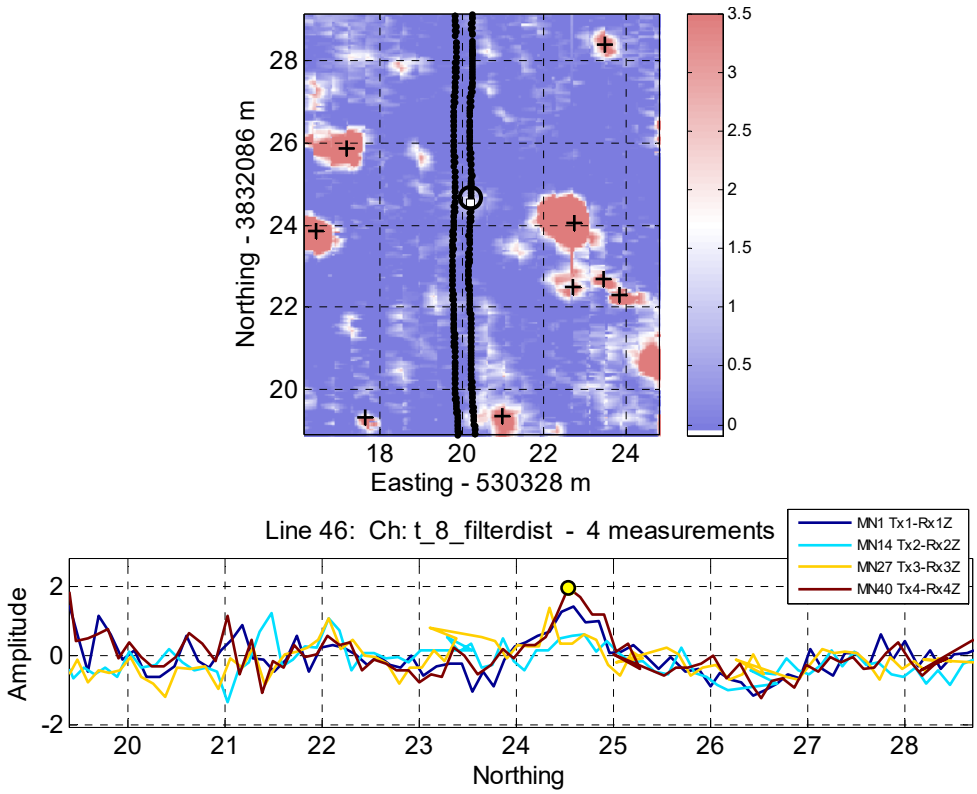

Figure 8. Along line profile TEMTADS data for Missed seed 1 (Grid G12). The monostatic (i.e. coaxial) z-component data for time channel 8 is shown. Circle is seed location. Yellow dot on line profile corresponds to seed location.

3.2.4.2 Missed seed 2. Grid H13 QA Seed V-3

This missed seed is a Medium ISO that was oriented vertically, at a depth of 0.46 m measured between the ground surface and top of ISO. The depth to the center of mass was 0.56 m. This seed was emplaced deeper than planned due to the hole having "opened up" (personal communication with Sandra Takata, CB&I). Figure 9(left) plots the co-axial, z-component data in the 8th time channel, using a maximum color scale of 5.9 mV/amp, which is the detection threshold for this grid. The seed location is indicated by an 'o'. Figure 9(right) and Figure 10 clearly shows that there is an anomaly associated with this seed, but its amplitude is below the picking threshold.

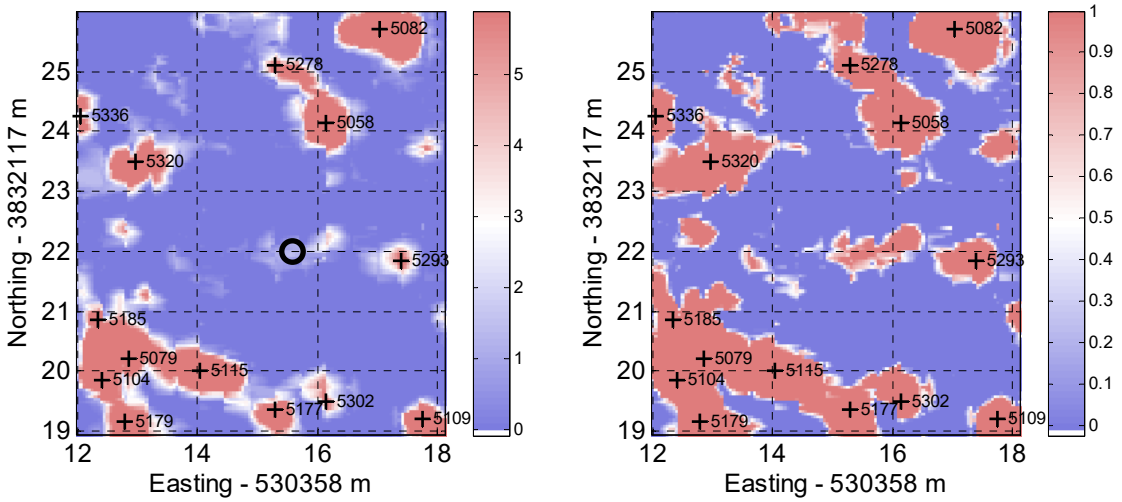

Figure 9. Gridded TEMTADS data for Missed seed 2 (grid H13). The monostatic (i.e. coaxial) z-component data for time channel 8 is shown.

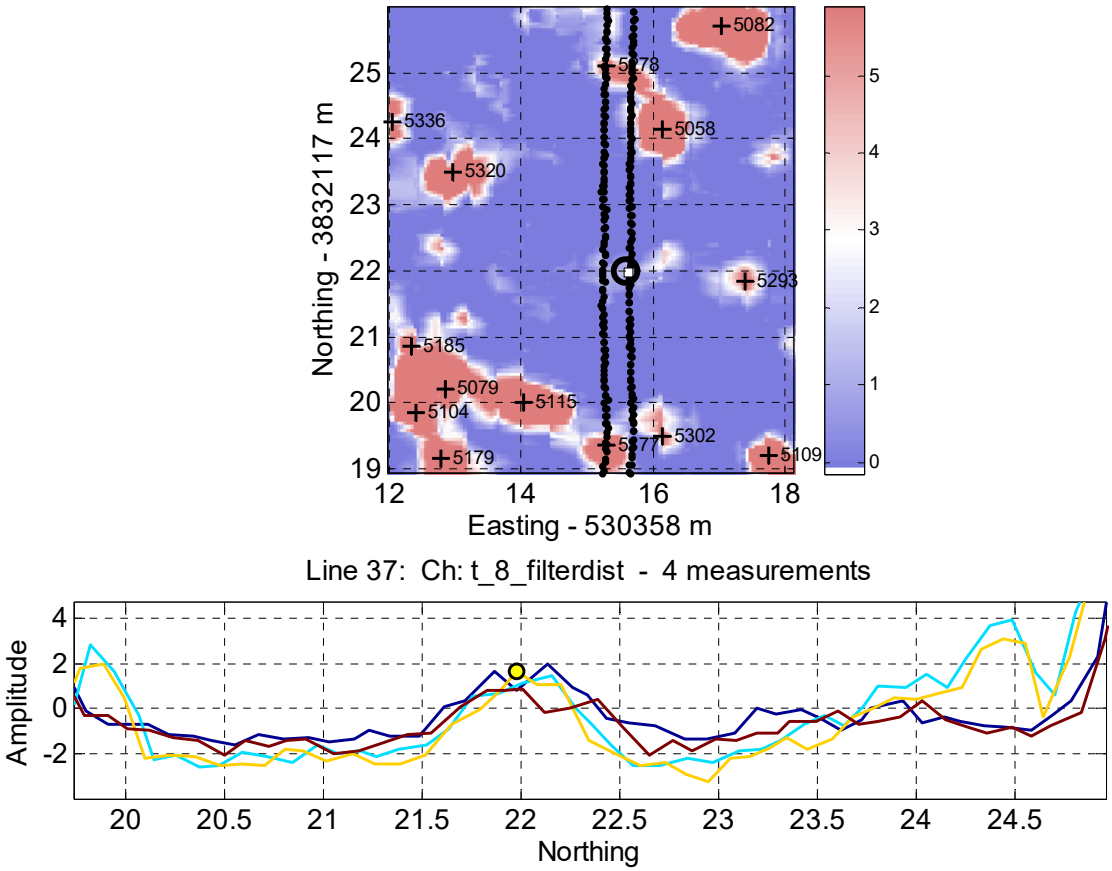

Figure 10. Along line profile TEMTADS data for Missed seed 2 (Grid H13). The monostatic (i.e. coaxial) z-component data for time channel 8 is shown. Circle is seed location. Yellow dot on line profile corresponds to seed location.

3.2.4.3 Missed seed 3. Grid B12 QC Seed

This seed did not have a target pick within the required 0.4 m location accuracy tolerance. The seed was a medium ISO at a depth of 0.3 m. Figure 10 marks the location of the QC seed with an 'x'. At this location, there is no corresponding data anomaly. It is not clear why this would be the case. The nearest target pick was located 0.45 m away from the seed (triangle in Figure 11). At this location, there is a data anomaly that exceeds the Grid B12 target picking threshold of 4.6 mV/amp. When this anomaly is inverted for a source location, a dipole source is predicted within the 0.4 m maximum radius from the seed location. In Figure 11 the dipole source is indicated by a 'o', which is 0.27 m from the seed location 'X'. This result suggests that anomalies in the dynamic TEMTADS data should be inverted for source locations to improve target picking positional accuracy.

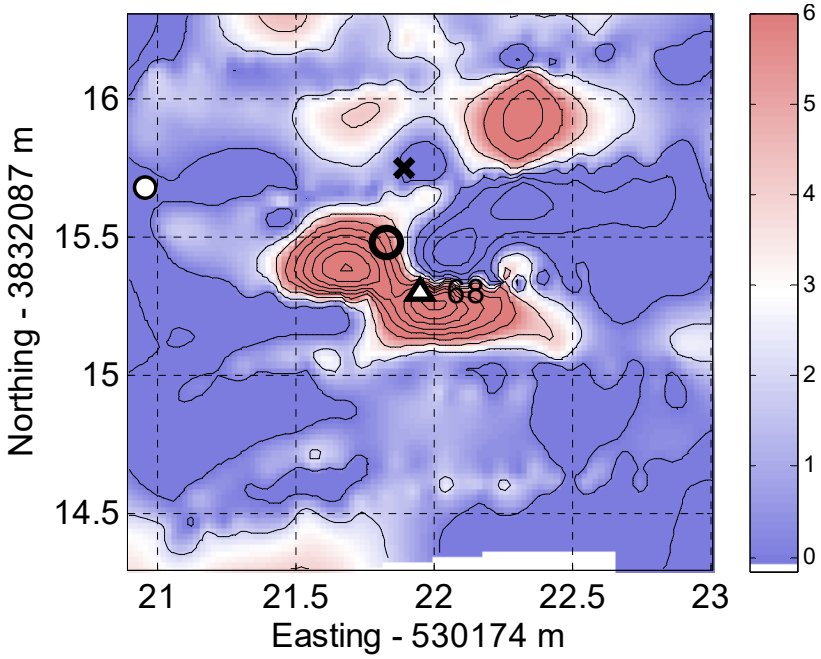

Figure 11. Gridded TEMTADS data for the missed QC seed in Grid B12. Triangle: initial pick location.

3.2.5 2.4 Corrective action for missed seeds (target selection)

Of the three seeds that were not included in the initial target picking lists, two were not reported due to issues related to the seed emplacement (i.e. incorrect ISO and incorrect depth). However, the QC seed in Grid B12 was missed due to inaccuracy of the data amplitude-based detection approach. The QC seed in Grid B12 would've been detected within the location accuracy tolerance if the anomaly was inverted, and the dipole source location was used for the target location. Therefore, the target picking approach was

modified so that every anomaly is inverted for dipole source locations. We note that the total number of anomalies typically decrease for each grid when using source locations instead of data anomalies, since multiple target picks can correspond to the same dipole source.

In addition to using source locations to improve target picking accuracy, it is also possible to use the inversion results to "screen out" targets that are unlikely to be targets of interest thereby reducing the number of cued interrogations required. For this project, we implemented a conservative source screening approach that identifies targets smaller than the smallest target of interest, i.e., an MK18 hand grenade. We note that the MK18 smoke grenade we are using for this analysis is thinner walled and produce a weaker response than the MK15 WP Smoke grenade (personal communication with Amy Walker). Using the larger MK15 WP Smoke grenade polarizabilities would result in more anomalies being screened out.

For each target pick, data were inverted to solve for one and two sources, for a total of 3 models per target. The "best" model was chosen as the one to use for the informed source selection (ISS) location. A set of rules were applied to find the "best" model for each target. E.g., if all models were located >0.4 m from the pick location, we used the pick location as the ISS location. Otherwise, models located >0.4 m from the pick location were omitted. We used a metric, *M*, based on size, decay and data and polarizabilities measures to determine which model to use. For a set of models, the model whose size, decay, data and polarizability properties are, overall, most typical of a TOI will have the highest M value. In some cases, a second object will be selected as a new target. For this to happen the second object must be >0.4 m from an existing target. The ISS locations for nearby targets frequently converge to the same point. The final step is to merge ISS locations that are within 0.4 m.

In our screening approach we compare the recovered total polarizability (i.e. the trace of the dipole polarizability tensor) to the minimum expected total polarizability for an MK18 hand grenade. The trace of the polarizability tensor is used rather than the eigenvalues, since the trace is a more robust value to estimate from noisy data.

The range of polarizabilities for a particular target type is a function of target depth and the data noise. The minimum expected total polarizability is determined for each grid using Monte Carlo type simulations. To achieve representative noise values for each grid, we artificially seeded targets in regions of each grid that do not have target picks. MK18 smoke grenade data were synthetically generated by assuming the target is at the maximum clearance depth. Each grenade wass given a random orientation, and the forward modeled data was then added to the leveled field data. To demonstrate this approach, we plot results

from applying the method to Grid L09. Figure 12 plots the leveled z-component, mono-static data from the 8th time channel before (left) and after (right) artificially seeding the MK18 hand grenade data in Grid L09.

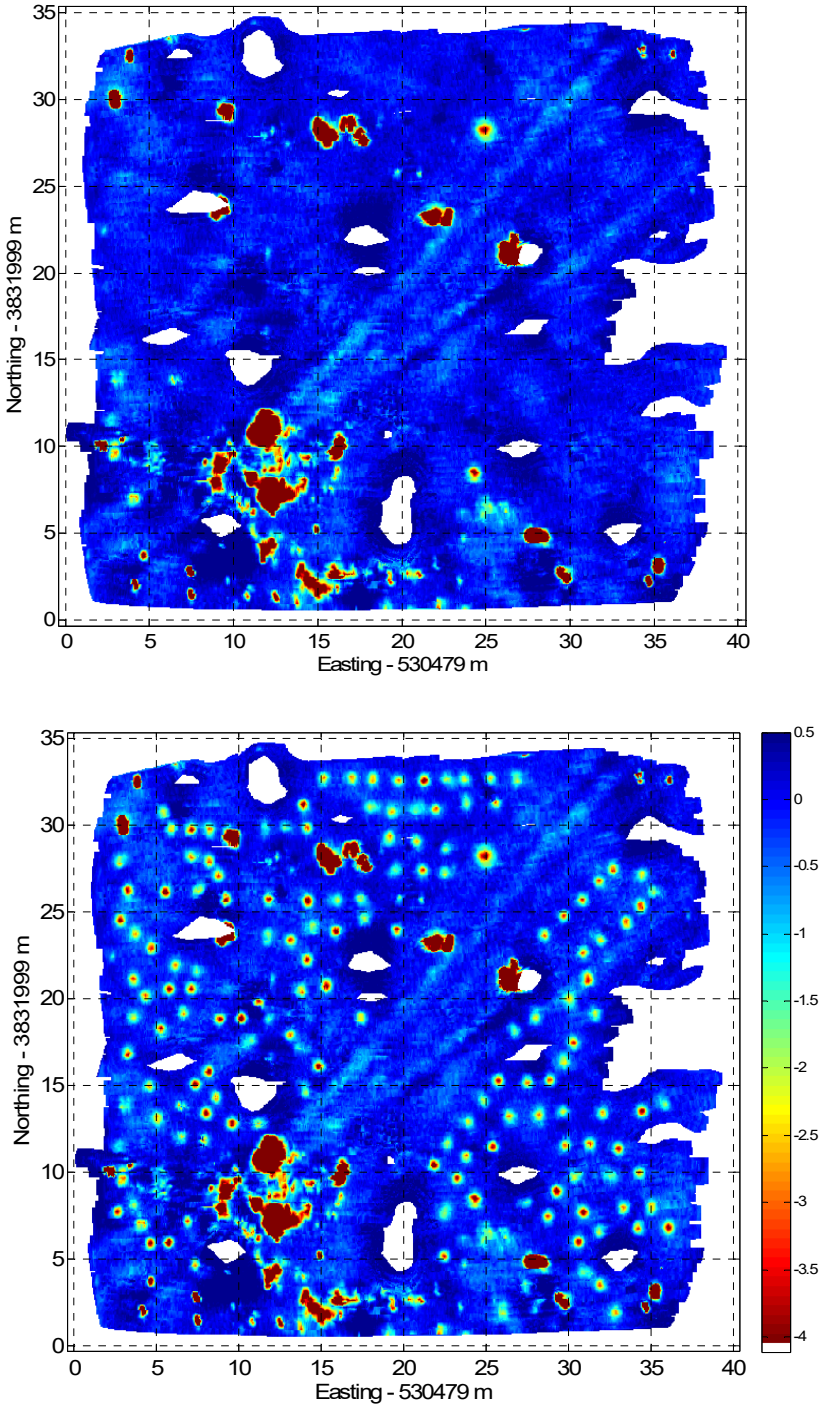

Figure 12. Example of artificially seeding a MK18 smoke grenade in a grid. For Grid L09, the seeded targets are buried at a depth of 0.36 m and are randomly oriented. The anomalies are subsequently inverted to determine the range of expected polarizabilities.

Each data anomaly from the artificially seeded target is inverted for a single dipole source. The collection of recovered polarizabilities is then examined to determine the lowest total polarizability expected to be found on the grid. Figure 13 shows the range of total polarizabilities when inverting artificially seeded data from Grid L09. The solid lines indicate the 6 total polarizability curves from the ESTCP library, and the dashed black line indicates the minimum polarizability expected for the grid. Any target with a polarizability less than this minimum polarizability is considered unlikely to be a target of interest.

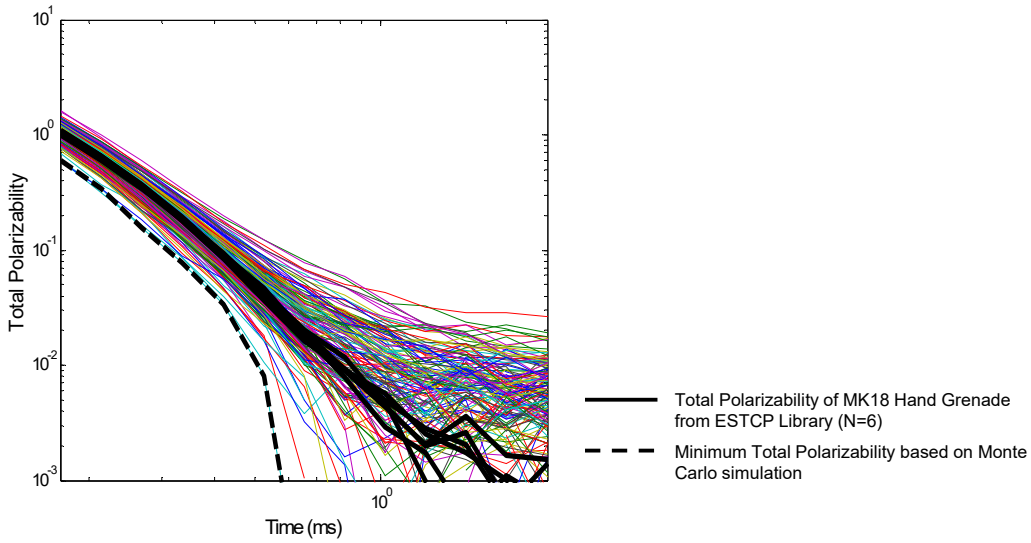

Figure 13. Recovered total polarizabilities of artificially seeded anomalies in grid L09. The recovered total polarizabilities are plotted in various colours, with the minimum total polarizability indicated by a black dashed line. The solid black lines show the 6 samples of total polarizabilities of the MK18 smoke grenade from the ESTCP Library.

Figure 14 compares the range of total polarizabilities from inverting Grid L09 data to the total polarizability of MK18 Smoke Grenades, the minimum total polarizability of the MK18 Smoke Grenade based on Monte Carlo simulation, a small ISO and a 20 mm projectile. Of the 99 anomalies picked in Grid L09, only 11 anomalies have polarizabilities smaller than the Mk18 smoke grenade threshold. The limited amount of screening is due to fast decay and relatively low amplitude of the MK18 smoke grenade polarizability curves. If, for example, screening was based on a larger TOI, such as a small ISO (green dashed line in Figure 14), significantly improved screening performance would be obtained. Indeed, the polarizabilities of the screened anomalies are smaller than the polarizabilities of the 20 mm projectile (red dashed line). Table 4 summarizes the screening results and final number of targets for each grid. Due to the high noise levels of grids N15 and H13, we decided the conservative approach would be to not apply the screening method, and to simply require a cued measurement for all anomalies in these grids. Target densities range between 459 targets/acre for grid L09 to 1133 targets per acre for grid H13.

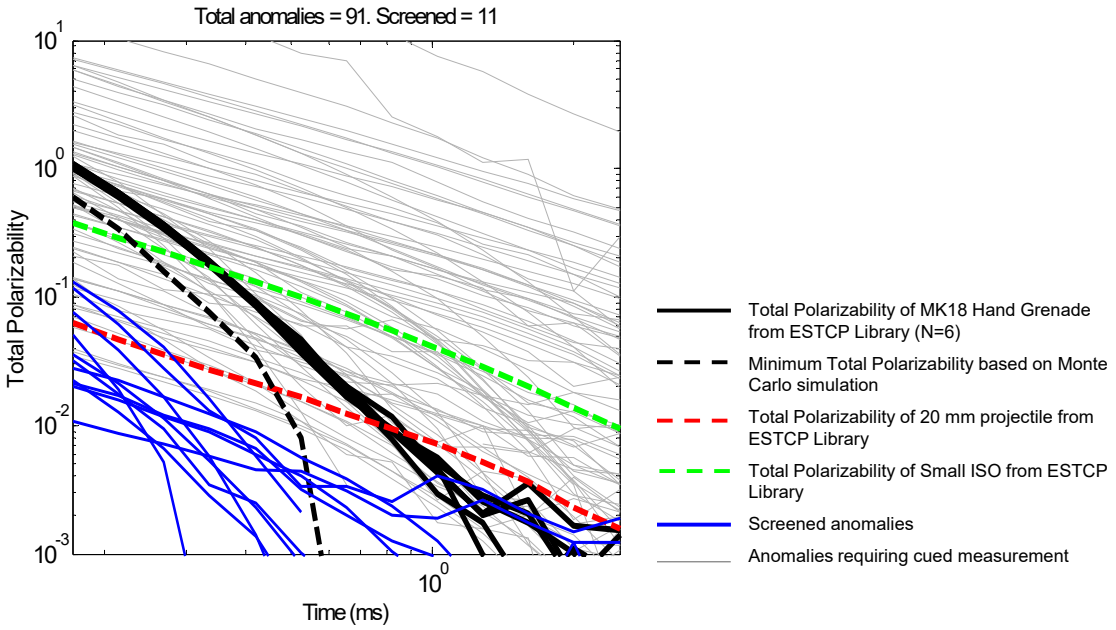

Figure 14. Comparison of estimated total polarizabilities to the minimum total polarizability estimated from Monte Carlo simulation.

Table 4. Number of anomalies screened, total number of anomalies including additional picks supplied by CB&I based on EM61 data, and approximate target densities for each grid. The screening approach was not applied to Grids N15 and H13 due to their high noise levels. Target densities do not include the EM61 picks.

Grid	Threshold (5 x MAD)	Number of screened anomalies	EM61 anomalies added by CB&I	Total number of anomalies	Target density (per acre)
R17 merged	1.3	17	28	164	716
L09	1.0	11	21	101	459
B12	4.6	4	0	148	650
N15	17.8	0	0	242	1099
G12	3.5	3	0	235	1005
H13	5.9	0	7	262	1133
J17	2.5	9	0	219	945
Total		**44**	**56**	**1371**	

3.2.6 Background locations

Approximately 15 potential background locations for each grid were selected manually from the gridded data. Locations were located in regions that appeared to be representative of the background response, with no nearby regions of elevated amplitude.

3.3 Cued data processing

Analysis of the data, including visual QC of data and inversion results, and dig list creation, was performed using the *UXOLab* software suite. No training digs were available; thus classification was performed with training data.

3.3.1 Background corrections

During import of cued data into UXOLab, backgrounds were assigned automatically based on distance and time (i.e., for each target, the closest background taken within two hours of the target acquisition was used). Of the 184 backgrounds acquired during the survey, 56 were classified as bad and not useable primarily due to an elevated response. For grids B12, H13, J17, L09 and R17 all targets had a good background taken within two hours. For grid G12 all but one target (4087) had a good background taken within two hours. For grid N15 58 targets have backgrounds taken more than two hours from the target acquisition.

3.3.2 Inversions

Cued data were inverted in *UXOLab* using a sequential inversion approach to estimate target location, depth and primary polarizabilities. Instrument height above the ground was assumed to be 22 cm. Noise standard deviation estimates were based on background measurements within a grid. Target location was constrained to lie between ±0.75 m in both X and Y directions relative to the acquisition location. Target depth was constrained to lie between –1.2 and 0 m. The initial optimization for target location identified up to eight starting models to input into the subsequent estimation of polarizabilities. Because of the difficulty in finding appropriate, representative background locations, we performed three sets of inversions for each target:

1. Data were inverted to solve for 1, 2 and 3 objects. Data were background corrected using the assigned background with no background scaling.
2. Data were inverted to solve for 1 and 2 objects. Data were background corrected using the assigned background data scaled by ×0.7.
3. Data were inverted to solve for 1 and 2 objects. Data were background corrected using the assigned background data scaled by ×1.1.

This was considered a conservative approach due to the uncertainty of the background response, which typically was large and variable within each grid. This resulted in a total of 12 models for each target.

3.3.3 QC of inversion results

Inversions with misfit values > 0.2 were failed and not used in the classification process. Models with an offset from the acquisition location of > 0.4 m were failed and not used in the classification process. Although it turned out that no training data were available prior to classification, targets were selected as training digs during QC.

3.3.4 Classification library

We used the ESTCP library created from recent test stand measurements. We used all library measurement made with the TEMTADS 2x2, the Portable Decoupled Electromagnetic Induction Sensor (PEDEMIS) system in a 3x3 configuration, and MetalMapper (Classic) using the long time window (24.38 ms). This library comprises 1641 items ranging in size from small land mines to very large (16 inch) projectiles. We augmented this library with 30 additional items, including three items measured in the Redstone test pit, four items from the Redstone IVS, and 23 items from our own classification library, for a total of 1671 library reference items.

3.3.5 Classification

Classification was performed by library matching using all three polarizabilities (L1 = primary, L2 = secondary, L3 = tertiary). The time channels used for calculating misfits with respect to the reference library varied from grid to grid based on an automated assessment of the polarizability quality (Table 5). Our library matching is based on polarizability misfit, so that smaller values represent better fits (0 represents a perfect fit). There is no upper bound on the misfit. The metric used for classification is 1/(polarizability misfit). The stop dig point for each grid was chosen by visual inspection of the polarizabilities in dig list order. Although no training digs were available, items were flagged as training (Table 5) and appear at the top of each submitted dig list.

Table 5. Summary of classification parameters. Targets is number of unique targets. “TOI” is a qualitative estimate of the number of targets that look like potential TOI. Training and “Can’t an.” are number of training digs and number of cannot analyze targets. Ch L1, L2 and L3 are the end time channels (ms) used when calculating polarizability misfits for the primary, secondary and tertiary polarizability, respectively. The start time channel for all misfits is channel 1 (0.117 ms). Digs is the total number of recommended digs (includes training and cannot-analyze digs). Stop metric is the metric at the chosen stop dig point. Last target is the target ID of the final dig.

Grid	Targets	"TOI"	Training	Can't analyze	Ch L1	Ch L2	Ch L3	Digs	Stop metric	Last target
B12	148	6	10	2	13.17	10.189	3.297	34	0.313	2206
G12	235	16	9	3	14.594	9.680	4.971	76	0.305	4238
H13	262	42	11	1	15.362	10.725	7.490	111	0.318	5043
J17	219	25	11	0	9.196	5.507	2.426	61	0.299	6238
L09	101	2	9	1	5.797	3.471	1.455	22	0.359	1160
N15	242	49	15	4	19.853	18.860	17.022	119	0.308	3082
R17	164	4	7	6	5.797	2.828	0.829	51	0.336	3

Total	**1371**	**144**	**72**	**17**				**474**		

3.4 Intrusive results

Due to a limited number of available ground truth digs, it was not possible to dig all items flagged as digs on the seven submitted dig lists. Instead, CB&I decided to dig a subset of targets identified manually by both BTG and CB&I to address the objectives of their program. This included digs both before and after the stop dig point on each list. Unfortunately, this means it is not possible to construct receiver operating characteristic (ROC) curves for the dig lists. Only a limited number of TOI per grid were dug (Table 6), some of which were challenging from a classification perspective. Below we look at the results for each TOI that was intrusively investigated.

Table 6. Summary of intrusive results. "# targets" is total number of unique targets in each grid. SDP is the stop dig point. "# dug" is the number of targets intrusively investigated. "# TOI dug" is the number of TOI included in the targets that were dug. "#TOI after SDP" is the number of TOI that appear after our stop dig point. *For grid N15, three digs were classified as PCWM, which we assume corresponds to TOI.

Grid	# targets	SDP	# dug	# TOI dug	# TOI after SDP
B12	148	34	36	1	0
G12	235	76	44	2	0
H13	262	111	42	1	1
J17	219	61	47	2	0
L09	101	22	24	2	0
N15	242	119	51	3*	2
R17	164	51	32	2	1

3.4.1.1 Grid B12 TOI

Target 2068, a medium ISO at 24 cm depth, was the only TOI dug in grid B12 (Figure 15). It occurred at dig #3 on our dig list because it was flagged for digging as a training item. If not flagged as a training dig, this seed would have been missed. The ISO was located almost exactly beneath the center of the sensor, and there is no indication in the provided ground truth information that any other metallic items nearby were found. Data fits are very good. Although the recovered polarizabilities do resemble those of a reference medium ISO, the second and third polarizabilities are poorly constrained leading to a large misfit value (0.732). At 24 cm depth, this item should have been easy to classify. With the information available, it is difficult to determine why this object did not produce a better result.

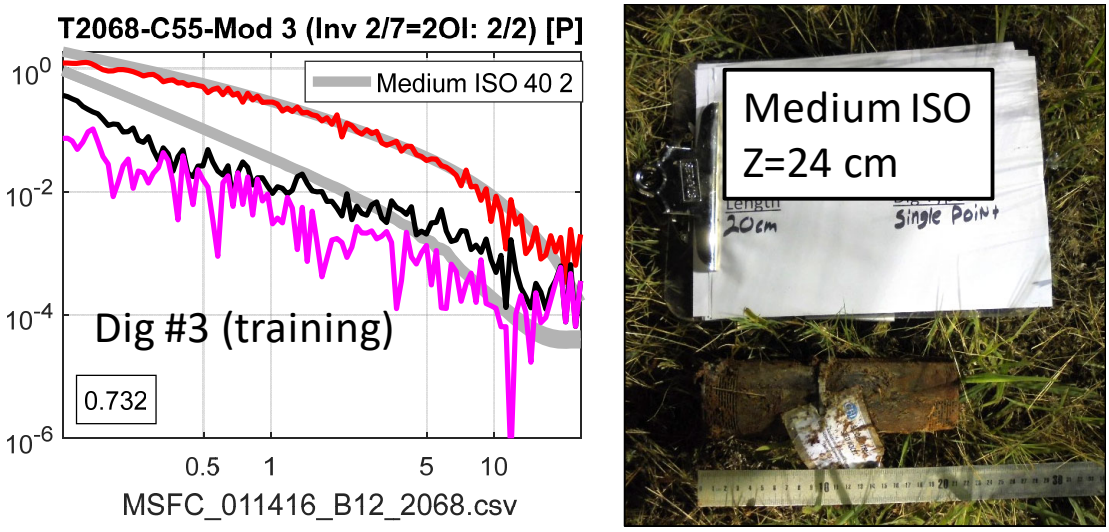

Figure 15. TOI in grid B12: target 2068, a medium ISO at depth of 24 cm.

3.4.1.2 Grid G12 TOI

Two medium ISO seeds, both at a depth of 27 cm, were dug in this grid (Figure 16). Both targets resulted in polarizabilities with good matches to a reference medium ISO and occurred well before the stop dig point on our grid G12 dig list.

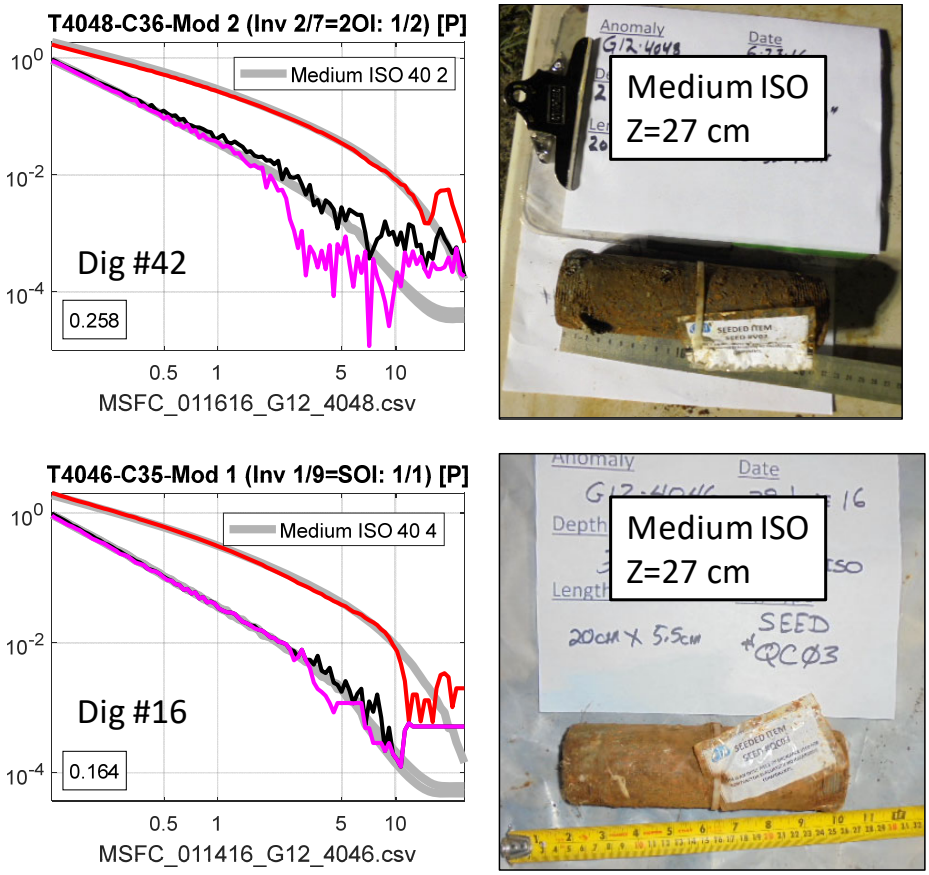

Figure 16. TOI in grid G12: (top) target 4048 and (bottom) target 4046. Both are medium ISOs at depth of 27 cm.

3.4.1.3 Grid H12 TOI

Target 5045 was a MEC item described as "det chord channel" at a depth of 23 cm (Figure 17). The reported location was ~1.5 m from the target pick location (and center of sensor). The reference ordnance library did not contain an entry for this one-off item and hence the reference item with the best fit (3.5" rocket) gave a relatively large misfit, resulting in this target appearing late on the dig list, after the stop dig point. Given the large offset and one-off nature of this TOI, it is understandable why this target did not appear as a dig on our dig list.

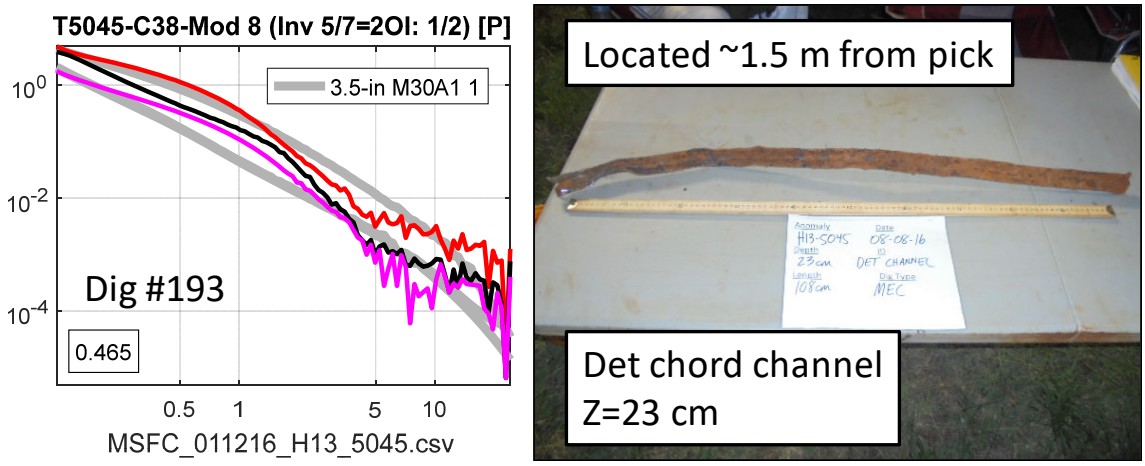

Figure 17. TOI in grid H12: target 5045, a MEC item described as "det chord channel" at depth of 23 cm. The reported ground truth location for this object was ~1.5 m from the target pick location and the location of the center of the sensor when this target was surveyed.

3.4.1.4 Grid J17 TOI

Two ISO seeds, a medium ISO at 25 cm and a large ISO at 52 cm, were dug in this grid (Figure 18). Both targets resulted in polarizabilities with good matches to their respective reference items and occurred well before the stop dig point on our grid J17 dig list.

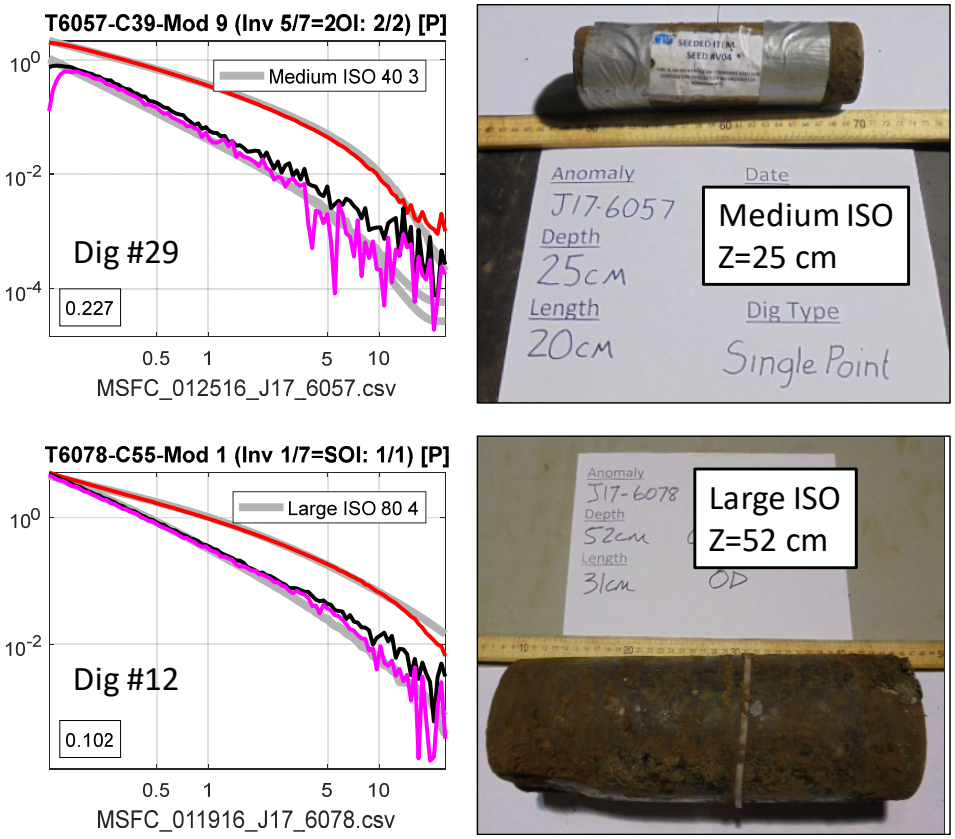

Figure 18. TOI in grid J17: (top) target 6057, a medium ISO at 25 cm depth; and (bottom) target 6078, a large ISO at depth of 52 cm.

3.4.1.5 Grid L09 TOI

Two ISO seeds, a medium ISO at 52 cm and a large ISO at 58 cm depth, were dug in this grid (Figure 19). At 52 cm, the medium ISO was well below the maximum depth for reliable classification, and this is reflected by the poor second and third polarizabilities. This item was flagged as a training dig and there occurred early (dig #5) on our dig list. If not flagged as a training dig, this item would have occurred late on the list.

The best fitting model to the large ISO resulted had noisy second and third polarizabilities; however, there was a model with a good fit to a 4" Stokes mortar (which is very similar in size to a large ISO) that had a good fit, resulting in this target appearing early on our dig list at dig #14.

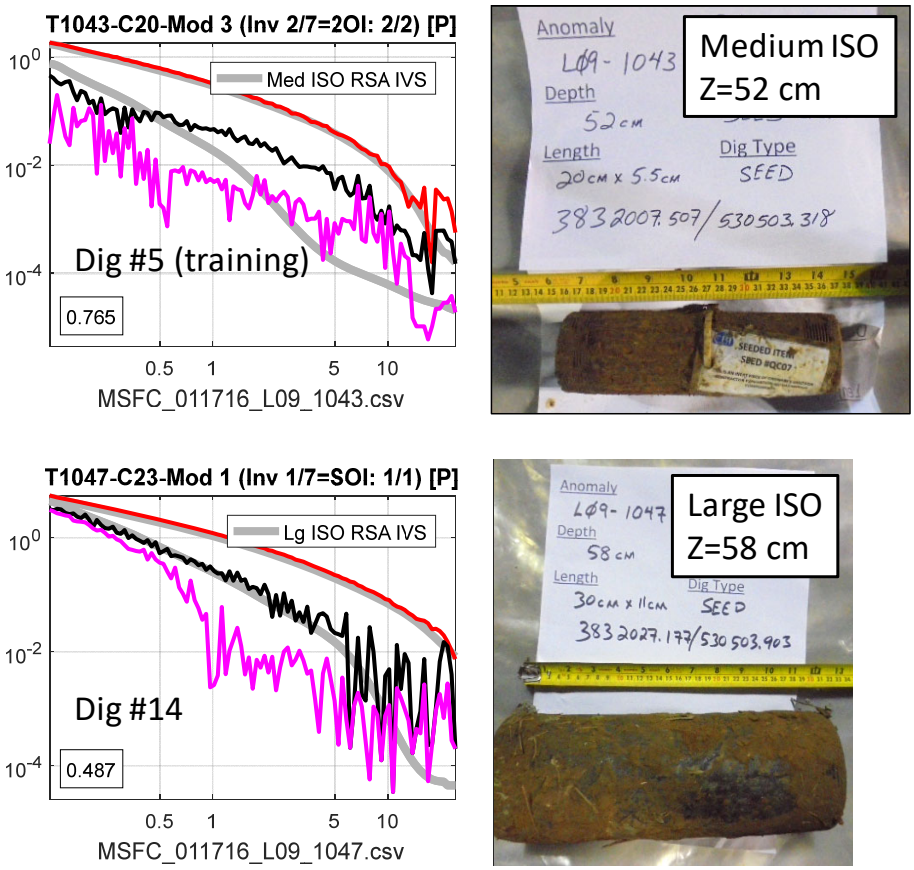

Figure 19. TOI in grid L09: (top) target 1043, a medium ISO at 52 cm depth; and (bottom) target 1047, a large ISO at depth of 58 cm.

3.4.1.6 Grid N15 TOI

Three TOI were dug in this grid: two 4.2” mortars at 18 and 48 cm depth, and a large M70 bomb at 110 cm depth (Figure 20). A large steel drum was found near the shallow 4.2” mortar, but the drum was 109 cm from the center of the sensor. Because the predicted polarizabilities are a good match to a 5” projectile, this target appear before the stop dig point on our dig list. A heavy steel 55-gallon drum and metal ring were found near the deeper medium ISO and were more proximal (40 cm offset) to the center of the sensor. Probably because of this, the predicted polarizabilities were degraded just enough to result in this target not being dug. In retrospect, the appearance of the polarizabilities should have resulted in this item being flagged as a training dig.

The M70 bomb was 77 cm from center of the sensor and very deep (110 cm), while three pieces of sheet/heavy metal and a metal bar were all closer to the sensor. The depth, large offset and presence of other more proximal pieces of large metal resulted in polarizabilities that do not have a good match to any of the reference items; hence this item was not included as a dig on our dig list.

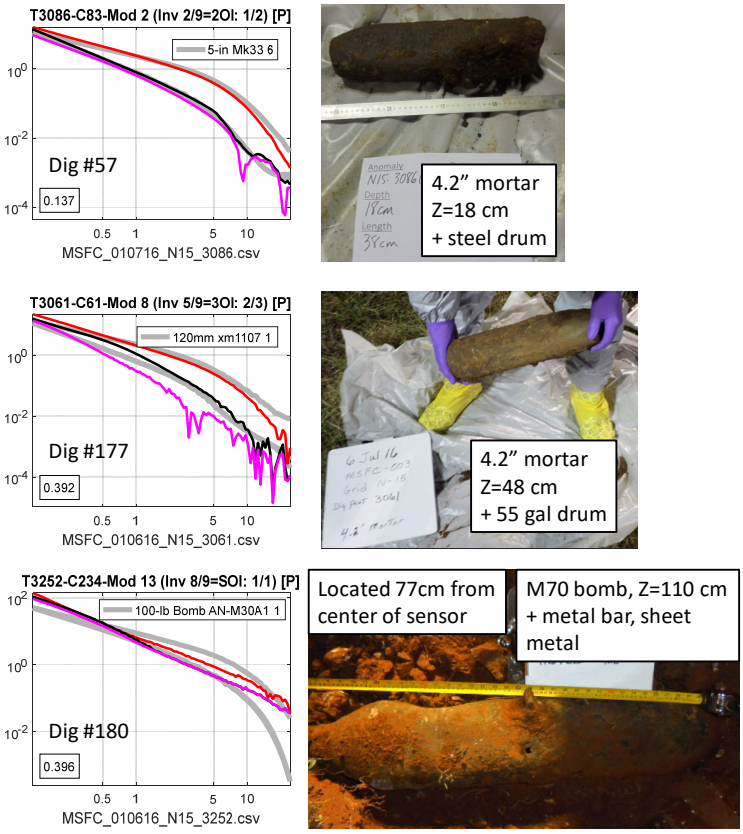

Figure 20. TOI in grid N15: (top) target 3086, a 4.2” mortar at 52 cm depth (with a steel drum); (center) target 3061, a 4.2” mortar at depth of 48 cm (with a 55-gallon drum); and (bottom) target 3252, an M70 bomb at 110 cm depth (with a metal bar and pieces of sheet metal).

3.4.1.7 Grid R17 TOI

Two seeds, a medium ISO at 50 cm and a large ISO at 45 cm depth, were dug in this grid (Figure 21). At 50 cm depth, the medium ISO was too deep for reliable classification. The predicted polarizabilities are very poor, resulting in this item occurring late on our dig list. The large ISO resulted in polarizabilities with a good match those from a reference large ISO, resulting in this target appearing early on our dig list.

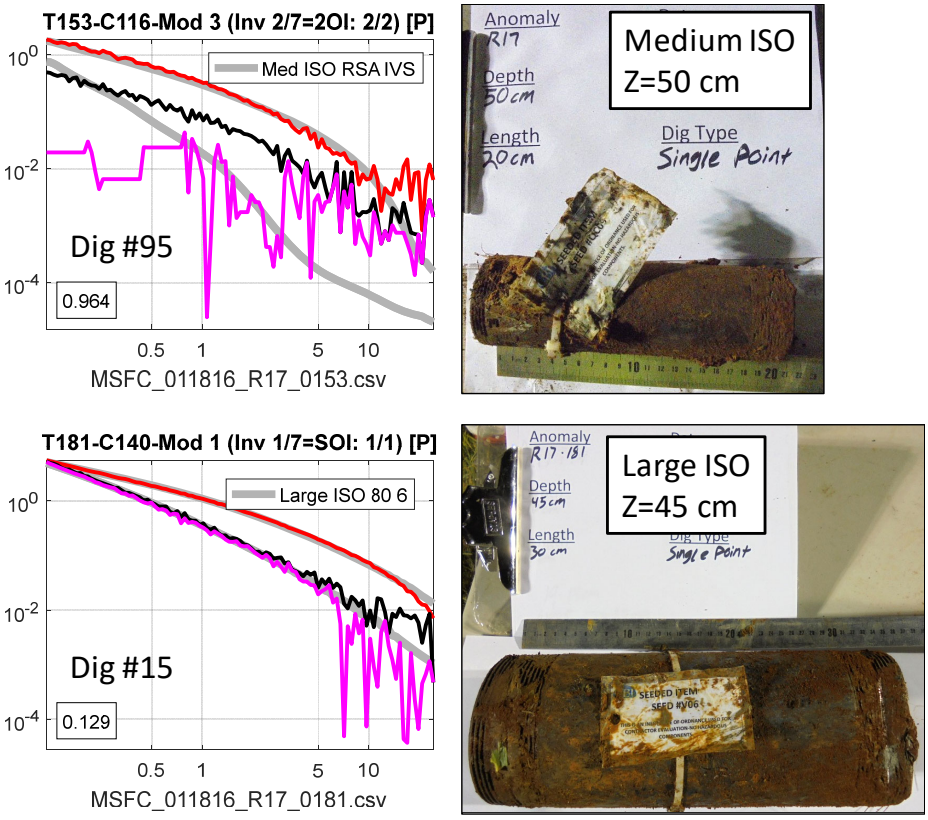

Figure 21. TOI in grid R17: (top) target 153, a medium ISO at 50 cm depth; and (bottom) target 181, a large ISO at 45 cm depth.

4 Appendix: Gridded dynamic data for each grid

Gridded data (monostatic Z-component; 8th time channel = 0.214 ms) for all seven grids. Black + symbols are target picks.

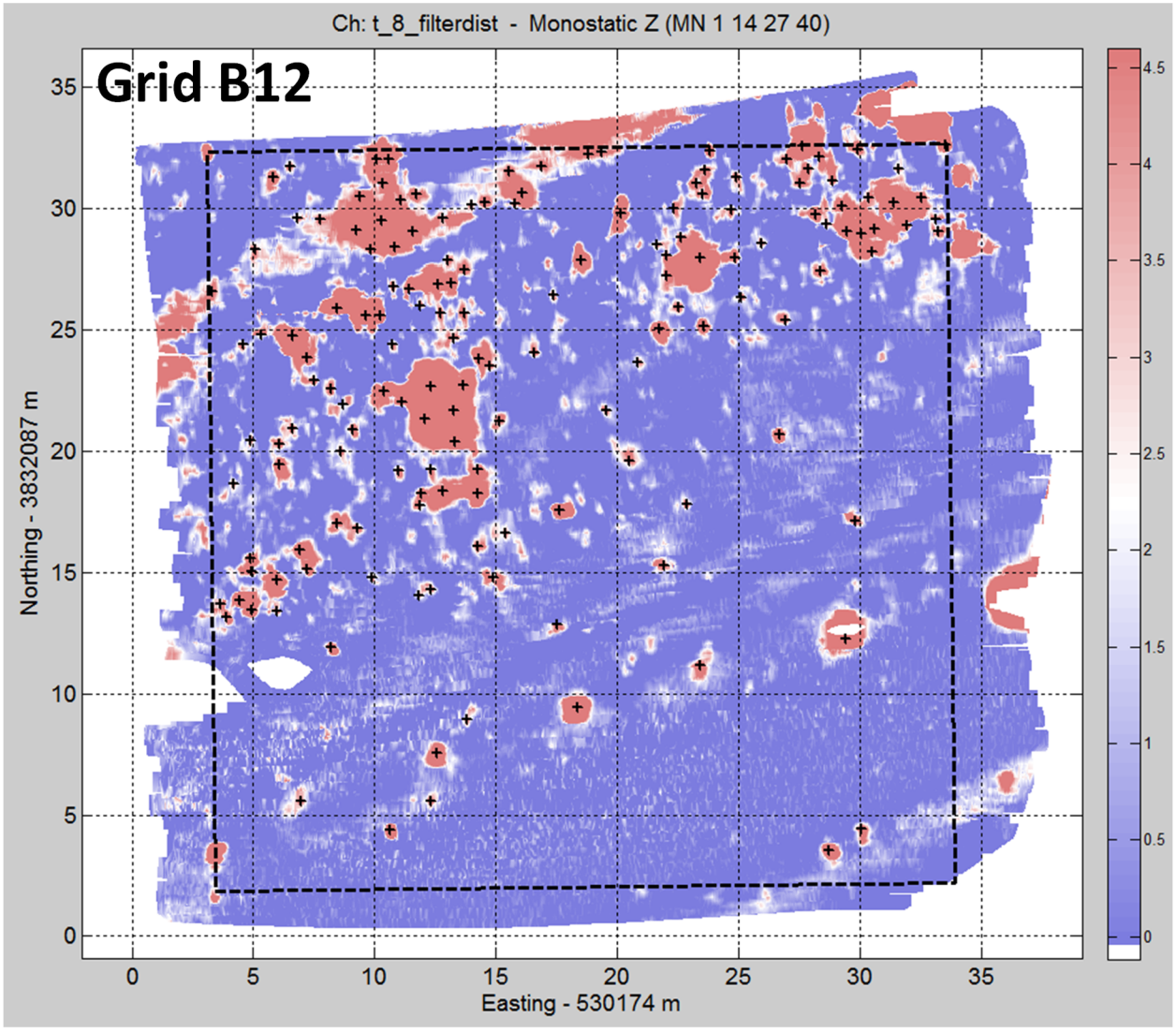

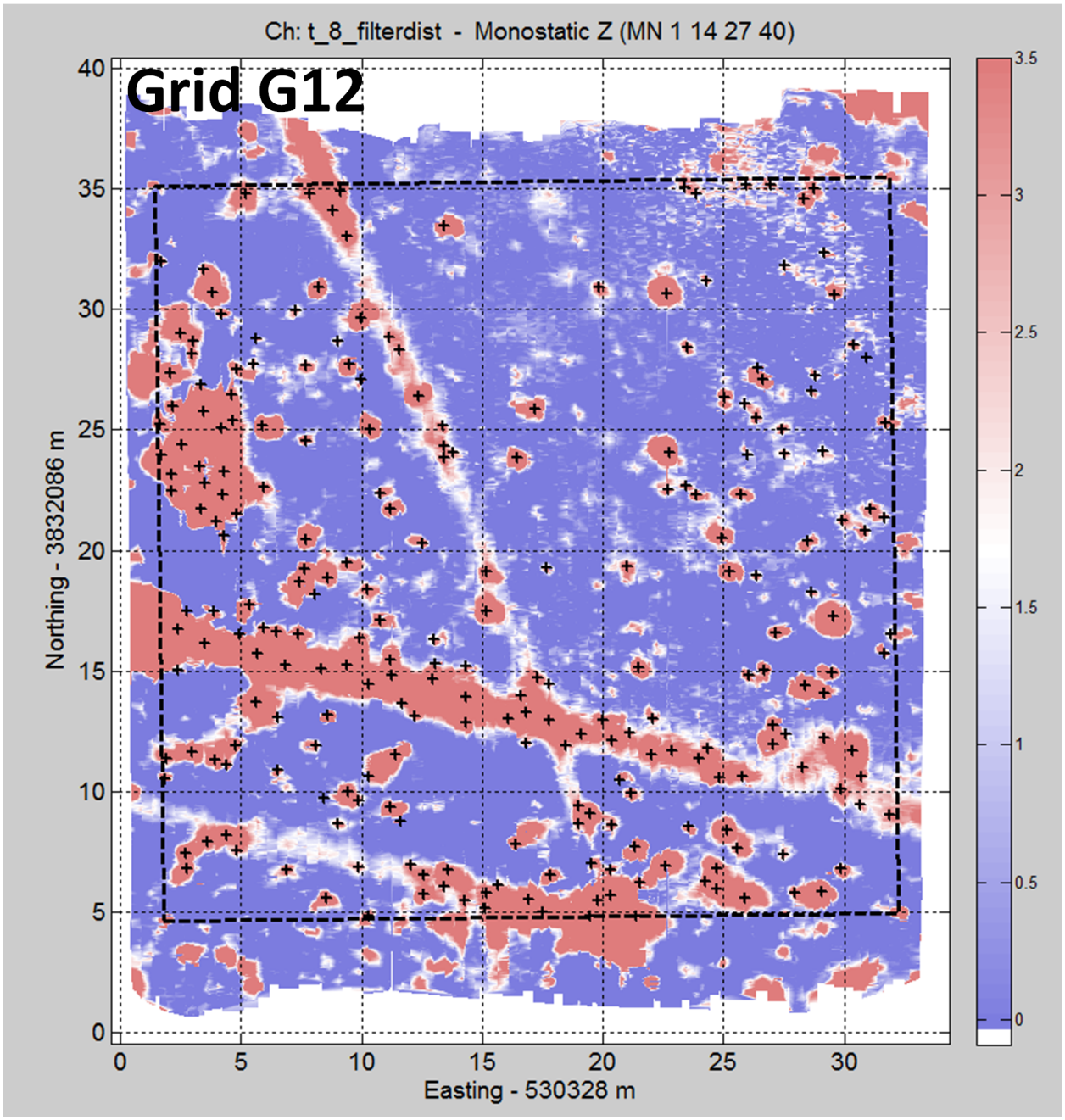
Ch: t_8_filterdist - Monostatic Z (MN 1 14 27 40)
Grid G12
Northing - 3832086 m
Easting - 530328 m
0
5
10
15
20
25
30
35
40
0
0.5
1
1.5
2
2.5
3
3.5

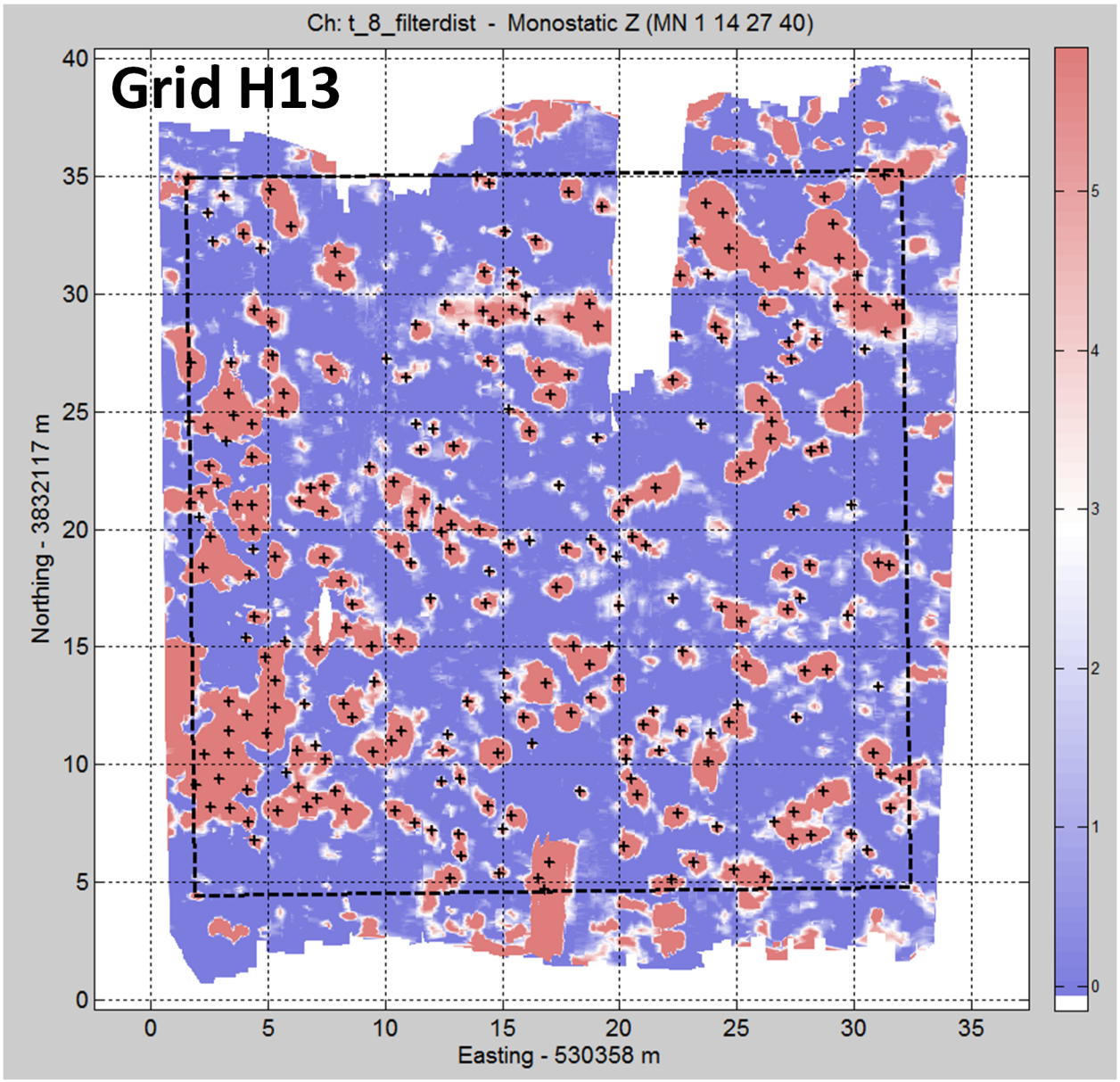
Ch: t_8_filterdist - Monostatic Z (MN 1 14 27 40)
Grid H13
Northing - 3832117 m
Easting - 530358 m
0
5
10
15
20
25
30
35
40
0
1
2
3
4
5

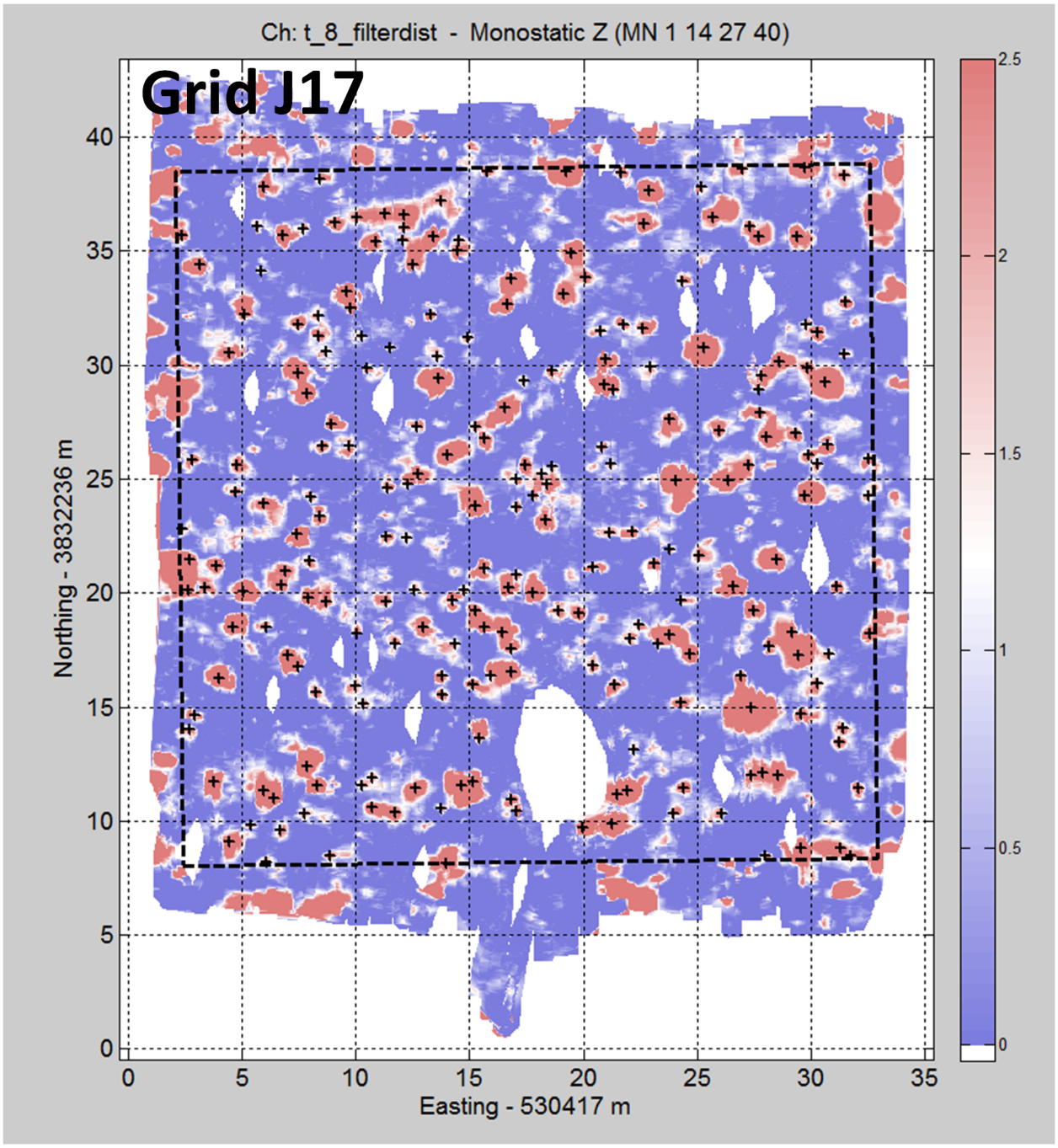
Ch: t_8_filterdist - Monostatic Z (MN 1 14 27 40)
Grid J17
Northing - 3832236 m
Easting - 530417 m
0
5
10
15
20
25
30
35
40
2.5
2
1.5
1
0.5
0

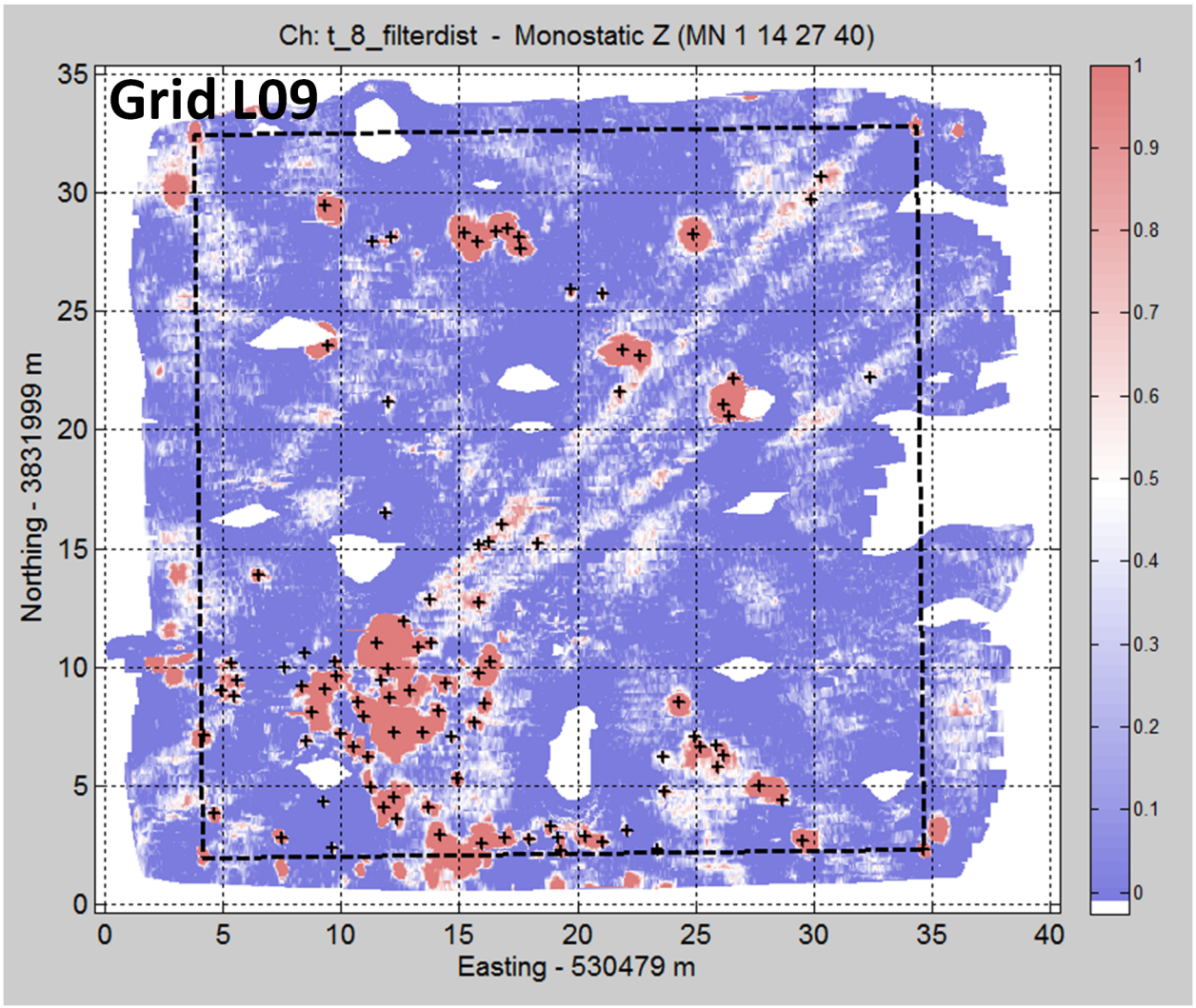
Ch: t_8_filterdist - Monostatic Z (MN 1 14 27 40)
Grid L09
Northing - 3831999 m
Easting - 530479 m
0
5
10
15
20
25
30
35
40
0.9
0.8
0.7
0.6
0.5
0.4
0.3
0.2
0.1

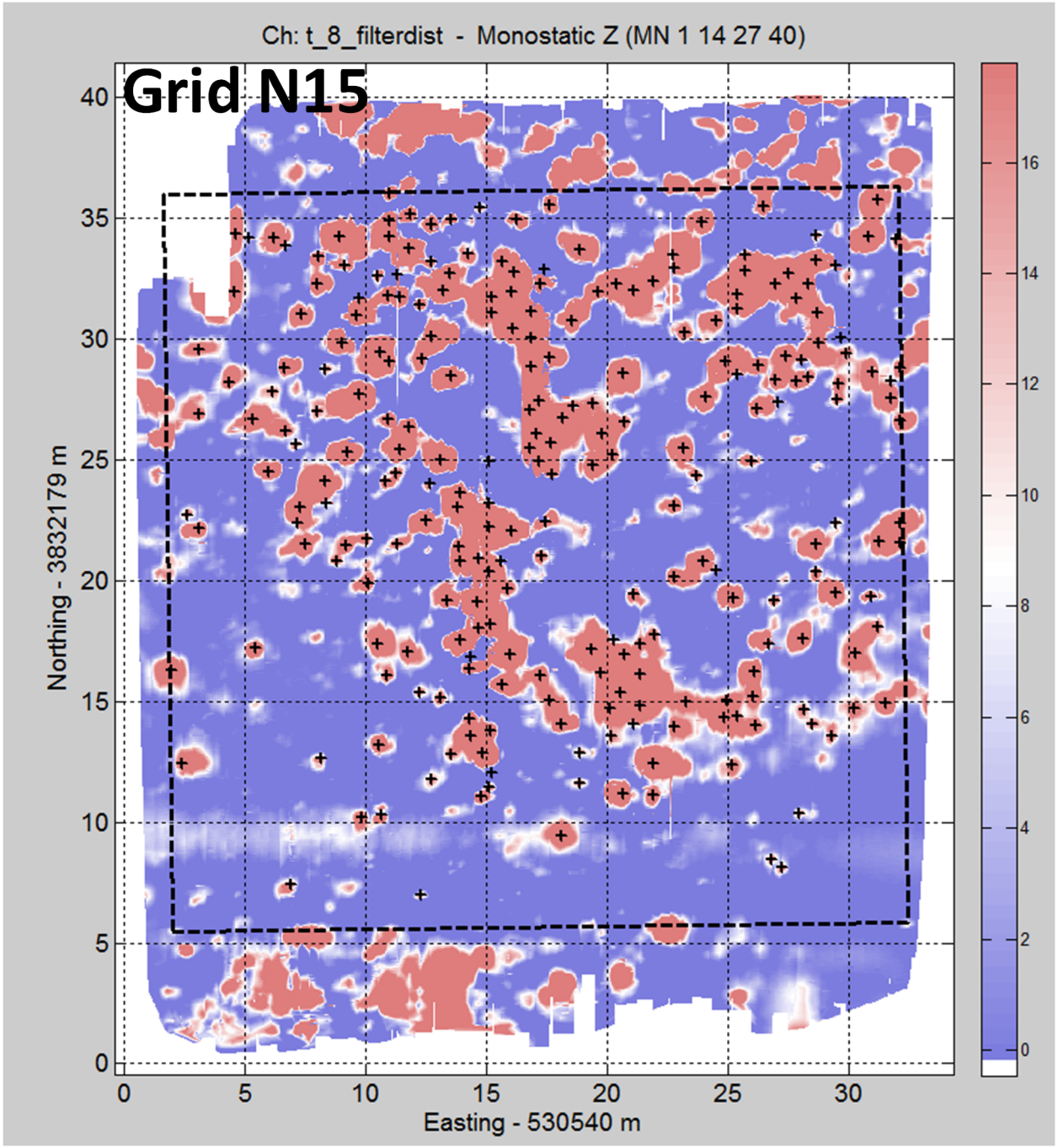
Ch: t_8_filterdist - Monostatic Z (MN 1 14 27 40)
Grid N15
Northing - 3832179 m
Easting - 530540 m
0
5
10
15
20
25
30
35
40
16
14
12
10
8
6
4
2
0

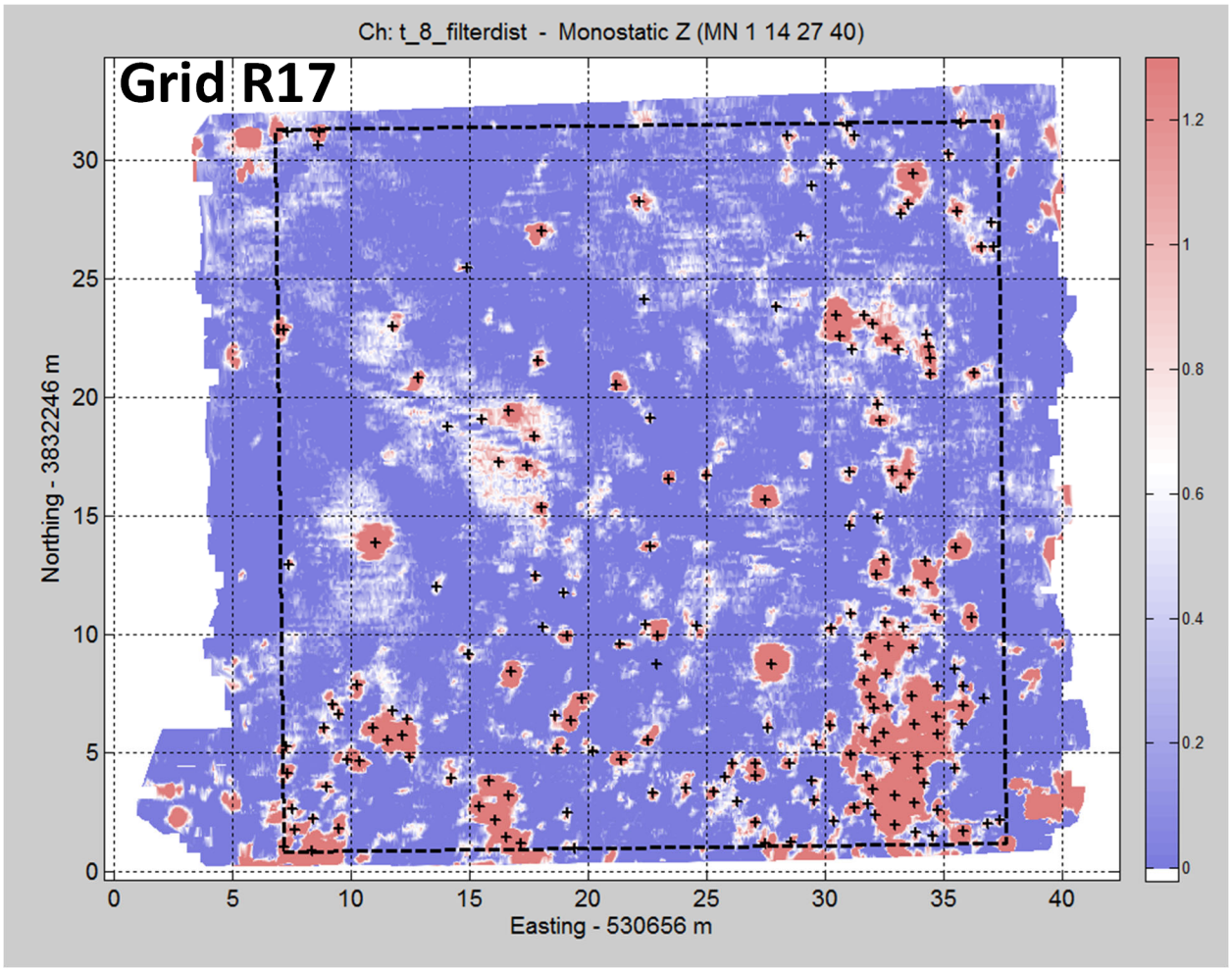
Ch: t_8_filterdist - Monostatic Z (MN 1 14 27 40)
Grid R17
Northing - 3832246 m
Easting - 530656 m
0
5
10
15
20
25
30
35
40
1.2
1
0.8
0.6
0.4
0.2
0